Renewable Energy Focus 50 (2024) 100582

Contents lists available at ScienceDirect

Renewable Energy Focus

journal homepage: www.journals.elsevier.com/renewable-energy-focus

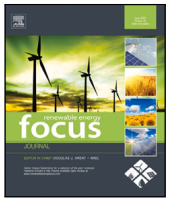

Research paper

The energy-balance method for optimal control in renewable energy applications

Chris Guiver [a,*], Mark R. Opmeer [b]

[a] School of Computing, Engineering & the Built Environment, Edinburgh Napier University, Merchiston Campus, Edinburgh, UK
[b] Department of Mathematical Sciences, University of Bath, Bath, UK

ARTICLE INFO

Keywords:
Linear graph modelling
Optimal control
Photovoltaic (PV) solar energy
Wave energy
Wind energy

ABSTRACT

A theoretical method is presented, called the energy-balance method, for maximising the energy extracted from a renewable energy converter in terms of determination of an optimal control. The method applies to control systems specified by linear graphs, and graph-theoretic techniques are employed. The method simplifies a number of optimal control problems by essentially expressing the performance objective — maximising energy extraction — in terms of an equivalent objective involving fewer variables, thereby reducing the complexity of the optimisation. As illustrated, in certain cases the optimal control problem may be reduced to one solvable by elementary calculus techniques. The theory is illustrated with examples from solar, wave and wind applications.

1. Introduction

The pressing requirement to decarbonise global electrical energy generation to reduce emissions and tackle the climate crisis is clear. Increased renewable energy conversion is one key mechanism to achieve this aim [1, p. 40]. Increasing renewable energy uptake over time has many facets, from political and regulatory, through to economic and technical. One economic consideration is reducing the Levelised Cost of Energy of a given renewable energy technology to attract commercial investment. This can be achieved by, for example, reducing the installation, operational and decommissioning costs of a given renewable energy device, or by increasing the energy converted over the lifetime of the device.

Here, we present a general theoretical method, which we call the *energy-balance method*, to solve the optimal control problem of maximal energy extraction by a renewable energy converter over a finite prediction interval. The method rewrites the original control problem, essentially by using Tellegen's theorem [2], in terms of a new performance objective which contains only a subset of the variables which appear in the original problem. Consequently, the resulting optimal control problem is no harder to solve than the original and is, in fact, often much simpler. Since optimal control problems can be challenging to solve analytically and numerically, methods which reduce the complexity of the problem are desirable. An important feature of our approach, and as shall become apparent, is to take a flexible view of the roles of variables, in the sense that (roughly) it is often more convenient to optimise a performance objective in terms of, say, a state variable in the original problem, and then use algebraic and/or differential equations — "the control system" — to *define* the remaining variables.

There are, of course, numerous mathematical and graphical descriptions of control systems. Presently, we employ a graph-theoretic representation of a control system, often called a *linear graph* in the engineering jargon; see, for example [3, Section 4.1] or [4, Chapter 5]. The graph determines the structure of the control system, where edges correspond to (lumped, one-port, two-terminal) elements in a given energy domain, and two variables are associated to each edge of the graph, called an across variable and a through variable. These variables are power conjugate and are also termed effort and flow variables in the literature. In electrical contexts, they correspond to voltages and currents, respectively. However, the linear graph framework permits treatment of control systems from other energy domains (mechanical translational, mechanical rotational, acoustic etc.), and the across and through variables satisfy certain algebraic relationships which are natural generalisations of Kirchoff's current law and Kirchoff's voltage law, respectively, as well as constitutive relationships on each edge, dependent on the element type.

As is well known, there is a choice of which variables in a given domain to assign as the across or through variables, often called *system analogies* (see, for example [5, Section 2]), and our treatment is independent of the chosen analogy. In all settings, the product of through and across variables is power. As we describe, the control systems we consider are assumed to comprise of a number of components, generalising resistors, capacitors, inductors and transformers/gyrators

* Corresponding author.
E-mail addresses: c.guiver@napier.ac.uk (C. Guiver), m.opmeer@bath.ac.uk (M.R. Opmeer).

https://doi.org/10.1016/j.ref.2024.100582
Received 29 June 2023; Accepted 3 May 2024
Available online 30 May 2024

as well as external sources and control terms, to the abstract setting. The inclusion of transducers facilitates modelling control systems which span multiple energy domains, such as mechatronic systems and so on [6,7]. We comment that a number of these components are permitted to be dynamic or nonlinear, and so are not necessarily ideal. As we illustrate in the examples considered, models for renewable energy generation via solar, wind and wave energy all fall within the scope of the control systems presented considered, and the energy-balance method is applicable.

The motivation for the present study is to simplify the procedure of determination of optimal controls in renewable energy applications. This aim resonates with a current direction in the control of wave energy converters, a timely and ongoing area of research, to *reduce* complexity [8, Section 3.3]. Furthermore, even if optimal controls are not implemented in the field, say because of robustness considerations or the real-time computational complexity, the energy generation of an optimal control provides a theoretical maximum against which other putative control schemes may be compared. Two strengths of our results are the following. First, the energy-balance method rewrites an optimal control problem as a simpler one, but is then agnostic to which optimisation or optimal control method is subsequently used, so this may be tailored to user preference or the bespoke setting. Classical optimal control techniques include so-called indirect methods such as the Pontryagin Principle (see, for example [9–11]) or Dynamic Programming (see, for example [12]), as well as so-called direct methods [13]. As we shall describe, in certain cases the energy-balance method reduces a dynamic- (or trajectory-) optimisation problem, that is, one subject to dynamic state constraints, to a static optimisation problem where no dynamic constraints apply. Here standard optimisation tools are applicable [14,15], such as gradient descent or nonlinear programming. Second, since the energy-balance method essentially works with the variables of energy, it applies to systems which span multiple energy domains, and so enables optimisation at a system-wide level.

The paper is organised as follows. Section 2 illustrates the main ideas behind the energy-balance method in a simple example. Sections 3 and 4 are the technical heart of the manuscript, and contain the graph theoretic ingredients required to specify control systems as so-called linear graphs and describe the energy-balance method, respectively. Sections Section 5, 6 and 7 contain applications of the method to renewable energy converters from solar, wind and wave energy contexts, respectively. Certain extensions to the energy-balance method and summarising remarks appear in Sections 8 and 9, respectively.

We comment that no single paper can thoroughly cover the three renewable energy application areas (solar, wave, wind) simultaneously, each of which is mature with its own academic and industrial/commercial communities. Rather, the main contribution of the present work is theoretical and is to present the energy-balance method in a focussed manner. The examples considered currently are primarily designed to illustrate how the energy-balance method applies, and hence how it is widely applicable. That written, in each case we demonstrate how known energy-maximising controls (such as maximum power point tracking — MPPT — for PV solar energy) naturally and straightforwardly arise from the energy-balance method, at least in simple settings. In depth studies in each particular application area shall constitute the focus of future works. Whilst there are numerous papers on the optimal control of renewable energy devices, such as those cited in Sections 5–7, we are not aware of a framework as general as that presented currently, at least for control systems specified by linear graphs.

2. The basic idea illustrated on a damped mass

We illustrate the basic ideas underpinning the energy-balance method through a simple example. Consider a damped mass m moving along a line with velocity $y = y(t)$ at time t and damping coefficient d on which an external force e acts and where power is taken off through a control force u:

$$m\dot{y} + d\,y = e - u\,. \tag{2.1}$$

The energy extracted over the time interval $[t_0, t_1]$ equals

$$\int_{t_0}^{t_1} y(t)u(t)\,\mathrm{d}t\,, \tag{2.2}$$

whereas the energy $E = E(t)$ in the system as time t is:

$$E(t) = \frac{m}{2}y(t)^2\,. \tag{2.3}$$

In practice the time interval $[t_0, t_1]$ is determined by our ability to predict the external force e; the length of this interval might be a few seconds. Maximising the energy extracted over this prediction interval is a natural optimal control problem, namely, how to design u. However, this optimal control problem tends to cause unwanted boundary effects since, as far as the optimal control is concerned, there is no time beyond t_1. We argue that a more sensible quantity to maximise over the prediction interval is:

$$E(t_1) - E(t_0) + \int_{t_0}^{t_1} y(t)u(t)\,\mathrm{d}t\,. \tag{2.4}$$

The integral term is as before and is the energy extracted over the prediction interval, whilst the term $E(t_1)-E(t_0)$ is the increase of energy stored in the system over the prediction interval. This stored energy is available for extraction at a later time. Indeed, since maximising the extracted energy over longer times requires piecing together multiple, successive prediction intervals (which is somewhat similar to model predictive control), the cost functional (2.4) seems appropriate.

Maximising (2.4) under the constraint (2.1) is another optimal control problem. Although traditional optimal control methods, such as the Pontryagin Principle can be used to determine an optimal control, these methods become extremely cumbersome for the more complicated problems studied later. In fact, since both the dynamics (2.1) and the cost function (2.4) are linear in the control u, this is (paradoxically) a hard problem because of the possibility of *singular control*, and traditional optimal control numerical methods have difficulties with nonlinear problems that are linear in the control; see, for example [13, Chapter 4]. Singular control, and the related situation of bang-singular-bang control (when constraints are present) are known to occur in the optimal control of wave energy devices [16].

Here, we utilise the additional structure of the problem which naturally comes from the renewable energy generation context to avoid the problem of singular control. In this section, we illustrate the method on the simple example (2.1) and (2.4), but its utility only really becomes clear in the more complicated examples considered later.

For our damped mass system, the following power balance:

$$\dot{E} = my\dot{y} = -dy^2 + ye - yu,$$

holds. Mathematically, we first differentiated (2.3) with respect to time and then utilised the differential equation (2.1). Integrating this over the time interval $[t_0, t_1]$ and re-arranging gives the following energy-balance:

$$E(t_1) - E(t_0) + \int_{t_0}^{t_1} y(t)u(t)\,\mathrm{d}t = \int_{t_0}^{t_1} y(t)e(t)\,\mathrm{d}t - \int_{t_0}^{t_1} d\,y(t)^2\,\mathrm{d}t\,. \tag{2.5}$$

An interpretation of the left-hand side of (2.5), which equals (2.3), has been given above. The right-hand side of (2.5) comprises two terms: the first

$$\int_{t_0}^{t_1} y(t)e(t)\,\mathrm{d}t,$$

equals the energy supplied over the interval $[t_0, t_1]$ by the external force e and the second

$$-\int_{t_0}^{t_1} d\,y(t)^2\,\mathrm{d}t,$$

is the energy dissipated over the interval $[t_0, t_1]$. Importantly, observe that maximising the left-hand side of (2.5) is equivalent to maximising the right-hand side of (2.5). We note that the right-hand side of (2.5) does not involve the control u. Consequently, the optimal control problem is trivially solved as follows. We maximise the integrand of the right-hand side of (2.5), that is, we maximise $y \mapsto ye - dy^2$, which gives $y = e/(2d)$. Therefore, the optimality condition we obtain is:

$$y(t) = \frac{1}{2d} e(t)\,. \tag{2.6}$$

The above formula is well known; see, for example [17, equation (6.44), p. 206] for a frequency domain expression, or [18, equation (2.12)]. The resulting optimal control goes by a number of terms, as discussed in [17, p. 206], such as *phase and amplitude control*, namely, the velocity of the mass being in phase with the excitation force with an appropriate amplitude, or *complex-conjugate control* (also known as impedance matching in electrical engineering).

To see which control achieves (2.6), we substitute this optimality condition into the differential equation (2.1) and obtain

$$u(t) = e(t) - m\dot{y}(t) - d\,y(t) = \frac{1}{2} e(t) - \frac{m}{2d}\dot{e}(t).$$

Therefore, the optimal control and optimal state are given in terms of the external force by:

$$u(t) = \frac{1}{2} e(t) - \frac{m}{2d}\dot{e}(t) \quad \text{and} \quad y(t) = \frac{1}{2d} e(t)\,. \tag{2.7}$$

Some remarks are in order. The crucial aspect of solution method is that the differential equation (2.1) is no longer viewed as a constraint, but as a *defining equation* for the optimal control u, in terms of the optimal state y and external force e. This is made possible by maximising the right-hand side of the energy-balance (2.5), which does not involve the control u, instead of maximising the left-hand side, which does involve u.

We also note that in this simple example, solving the optimal control problem was trivial. As we shall see, this will not always be the case but, when applicable, the energy-balance method we present reduces the complexity of the optimal control problem to be solved. We have not included input- or state-constraints here, which of course will feature in real-world applications, and we comment on how constraints may be included in Section 8.

3. Graph-theoretic modelling of control systems

In order to generalise the method outlined in Section 2, we shall view control systems from a graph-theoretic perspective and the current section gathers the requisite material. These objects are often called *linear graphs* in engineering contexts; see, for example [3, Section 2.1]. Treatments of control systems as linear graphs appear across older works, such as [19–21], with [4] a recent text. We refer the reader to these texts for further background on writing control systems as linear graphs.

3.1. Planar and dual graphs

We collect the requisite graph-theoretic notation and terminology. We consider a finite directed graph without self-loops, and with possibly multiple edges between the same pair of vertices. This can be formally described by a triple $(\mathcal{V}, \mathcal{E}, \alpha)$ where $\mathcal{V}$ is the finite set of vertices (also called nodes), $\mathcal{E}$ is the finite set of edges (also called branches in some texts) and

$$\alpha : \mathcal{E} \to \{(x, y) \in \mathcal{V} \times \mathcal{V} : x \neq y\},$$

is the *incidence function*. The calligraphic notation for the vertices $\mathcal{V}$ and edges $\mathcal{E}$ is to distinguish these objects from voltages V and energies E which commonly occur elsewhere.

When we draw a graph in the plane, we draw vertices as circles, edges as line segments and we draw an arrow on the edge e from x to y if $\alpha(e) = (x, y)$. In what follows, the directions on the edges are simply to fix signs and otherwise have no physical meaning. Two examples of graphs are shown in Fig. 3.1.

The graphs we consider can always be drawn in the plane, meaning they can be drawn without edges crossing, and such graphs are called *planar*. We specify a particular embedding in the plane by drawing a figure; this makes our graph into a *plane graph*. That we consider plane graphs is really only of importance when we consider duality. Our graphs will always be *connected* (here ignoring directions, meaning that the underlying graph of our directed graph is connected). We will denote the number of vertices by n and the number of edges by m. From Euler's formula for plane graphs (see, for example [22, Theorem 15, p. 22]), such a graph then has $m - n + 2$ faces, including the unbounded face.

We will relate matrices and vectors to our graphs. For this, we order the edges and vertex sets by writing $\mathcal{E} = \{1, \ldots, m\}$ and $\mathcal{V} = \{1, \ldots, n\}$.

The *incidence matrix* $\mathcal{M}$ of a graph is the $n \times m$ matrix which has

$\mathcal{M}_{ij} = 1$ if edge j starts at vertex i

$\mathcal{M}_{ij} = -1$ if edge j ends at vertex i, and

$\mathcal{M}_{ij} = 0$ if edge j is not incident to vertex i.

The *face matrix* $\mathcal{F}$ of a plane graph is a $(m-n+2)\times m$ matrix which has

$\mathcal{F}_{ij} = 1$ if edge j bounds face i and is oriented counter-clockwise with respect to the face

$\mathcal{F}_{ij} = -1$ if edge j bounds face i and is oriented clockwise, and

$\mathcal{F}_{ij} = 0$ if edge j does not bound face i.

Here oriented counter-clockwise means that the face is on the left of the edge as it is traversed along the direction of the arrow, and oriented clockwise means the face is on the right of the edge.

We note that the face matrix is a special cycle matrix and, apart from when used for duality, could in what comes below be replaced by a general cycle matrix. Since each edge bounds exactly two faces, and with opposite orientation, the face matrix $\mathcal{F}$ is itself the incidence matrix of a graph, called the *dual graph*. From a drawing of the graph, we can obtain a drawing of the dual graph as follows: in each face draw a dual vertex and connect dual vertices by a dual edge if the corresponding (primal) faces share a (primal) edge.

We consider an example.

Example 3.1. Consider the graph drawn in Fig. 3.1(a) with edges and vertices labelled. The incidence matrix for this graph is

$$\mathcal{M} = \begin{pmatrix} 1 & 0 & 0 & 0 & 0 & -1 & 0 & 0 \\ 0 & 0 & 0 & 0 & -1 & 1 & 0 & 0 \\ -1 & -1 & 0 & 0 & 0 & 0 & 0 & -1 \\ 0 & 0 & 0 & 0 & 0 & 0 & -1 & 1 \\ 0 & 0 & 0 & 1 & 1 & 0 & 1 & 0 \\ 0 & 1 & -1 & 0 & 0 & 0 & 0 & 0 \\ 0 & 0 & 1 & -1 & 0 & 0 & 0 & 0 \end{pmatrix}.$$

Fixing the following ordering of faces: upper bounded face, lower bounded face, unbounded face; the face matrix of the graph in Fig. 3.1(a) is

$$\mathcal{F} = \begin{pmatrix} 1 & 0 & 0 & 0 & 1 & 1 & -1 & -1 \\ 0 & -1 & -1 & -1 & 0 & 0 & 1 & 1 \\ -1 & 1 & 1 & 1 & -1 & -1 & 0 & 0 \end{pmatrix}.$$

This is the incidence matrix of the graph in Fig. 3.1(b) which is, therefore, the dual graph of the graph in Fig. 3.1(a). □

Presently, duality is introduced and used as follows. When modelling control systems as linear graphs, a so-called *systems analogy* [5, Section 2.1] must be chosen which, mathematically, prescribes algebraic conditions, determined by a graph, on pairs of power-conjugate

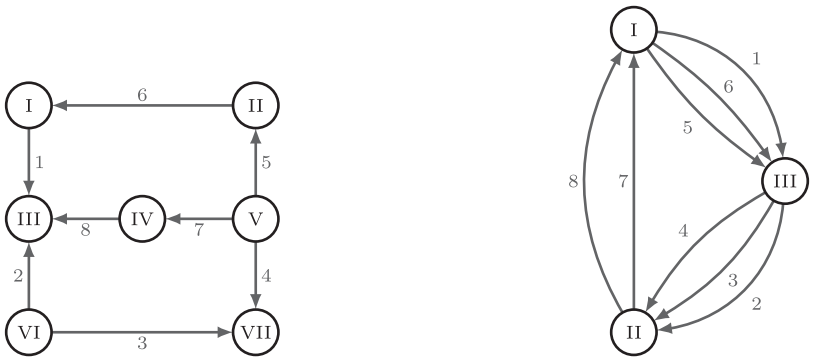

(a) Planar graph (b) The dual graph

Fig. 3.1. Examples of plane graphs.

variables associated with each edge of the graph. The algebraic conditions on the pairs of variables in each analogy are dual, in the sense that the primal graph in one analogy is the dual graph in the other. Therefore, duality permits straightforward conversion between analogies. Being able to convert between analogies becomes essential when seeking to merge linear graphs from different domains (electrical, translational/rotational mechanical, acoustic etc.) where different analogies may be preferentially used.

3.2. Functions on graphs

Given a planar graph as in the previous subsection, we will identify a function $f : \mathcal{E} \to \mathbb{R}$ defined on the edges of a graph with a vector in $\mathbb{R}^m$ and will identify a function $\phi : \mathcal{V} \to \mathbb{R}$ defined on the vertices of a graph with a vector in $\mathbb{R}^n$.

An edge function f is called *across* if $\mathcal{F}f = 0$. This is equivalent to the existence of a *potential* vertex function ϕ such that $f = \mathcal{M}^\top \phi$. The potential ϕ is unique if at a specified vertex i the condition $\phi(i) = 0$ is imposed (in electrical engineering terms, the vertex i can be considered *ground*). We call the components of an across edge function *across variables*, although the terminology generalised across variables also appears in the literature. Intuitively, across variables are those which are measured "across" the two terminals of a one-port element. In words, the condition $\mathcal{F}f = 0$ states that the across variables sum to zero around faces, or directed loops, and is called the compatibility law in [3, Section 4.3] and the loop rule in [6, Section 4.3].

An edge function f is called *through* if $\mathcal{M}f = 0$ and the components of a through edge function are called *through variables*. As before, the terminology generalised through variables is also used in the literature. Intuitively, through variables are those which act "through" the element. In words, the condition $\mathcal{M}f = 0$ states that the directed sum of through variables at every vertex equals zero. The condition $\mathcal{M}f = 0$ is called the continuity law in [3, Section 4.3] and the nodal rule in [6, Section 4.3].

We note that a function which is across for a (primal) graph is through for the dual graph, and vice versa.

Since $\mathcal{F}$ and $\mathcal{M}$ are both rank deficient by one, the across and through conditions give

$$n + (m - n + 2) - 2 = m,$$

independent equations for the $2m$ scalar unknowns contained in two (generally distinct) edge functions. Hence, by additionally specifying for each edge a single equation relating the two functions, we obtain in total $2m$ equations, which generically gives existence and uniqueness of an across edge function and a through edge function on a planar graph.

The edge functions we consider presently will typically depend on time as well, meaning that the components of the corresponding vectors in $\mathbb{R}^m$ or $\mathbb{R}^n$ are themselves functions of a real variable, and the across/through equations are assumed to hold pointwise in time. Consequently, across/through variables are functions of time in this case.

3.3. Control systems as graphs

On our graphs, we consider a pair of edge functions, one being across and one being through. The canonical example of an across function is voltage, and the across condition is Kirchhoff's voltage law. Similarly, the canonical example of a through function is current, and the through condition is Kirchhoff's current law. Intuitively, the product of a through variable and an across variable is *power*, the time derivative of *energy*. As such, we model control systems in terms of power conjugate variables, as in [5, Section 2.1].

For each of the edges we will have one (and only one) of the following possibilities:

- A *through-accumulator*. Here the energy E stored on the edge is a function of an auxiliary variable x, and the through variable T and across variable A satisfy

  $$T = \frac{\partial E}{\partial x}, \qquad \dot{x} = A.$$

  The typical situation is where E is quadratic: $E(x) = x^2/(2L)$ for L a positive constant, so that

  $$T = \frac{x}{L}, \qquad \dot{x} = A,$$

  and the auxiliary function x can be eliminated to obtain

  $$L\dot{T} = A.$$

  The energy is then given by $E = LT^2/2$, hence the terminology through-accumulator — the energy is stored in the through variable. A through accumulator is called a *T-type energy storage element* in [3, Section 3.3].
- An *across-accumulator*. Here the energy E stored on the edge is a function of an auxiliary function x, and the through variable T and across variable A satisfy

  $$A = \frac{\partial E}{\partial x}, \qquad \dot{x} = T.$$

  The typical situation is where E is quadratic: $E(x) = x^2/(2C)$ for C a positive constant, so that

  $$A = \frac{x}{C}, \qquad \dot{x} = T,$$

  and the auxiliary function x can be eliminated to obtain

  $$C\dot{A} = T.$$

  Correspondingly, the energy is then given by $E = CA^2/2$, hence the terminology across-accumulator — the energy is stored in the across variable. An across accumulator is called an *A-type energy storage element* in [3, Section 3.3].
- A *dissipator*. We consider three different types. Let $\{X, Y\} = \{A, T\}$, so that X and Y are placeholders for A and T, in some combination.

  - A linear dissipator: $X = RY$, where $R > 0$ is a constant.
  - A nonlinear dissipator $X = r(Y)$, where $r : \mathbb{R} \to \mathbb{R}$ and $r(Y)Y \geq 0$.
  - A dynamic dissipator. Here there is an auxiliary (vector-valued) variable z which satisfies

    $$\dot{z} = Fz + GX, \qquad Y = Hz + JX,$$

    where the transfer function of the above linear control system is assumed to be positive real, that is, with

    $$\mathbf{G}(s) = H(sI - F)^{-1}G + J,$$

    we have that $\mathbf{G}$ is holomorphic on $\{s : \mathrm{Re}(s) > 0\}$ and $\mathbf{G}(s)^* + \mathbf{G}(s) \geq 0$ for all s with $\mathrm{Re}(s) > 0$; see, for example [23].

  We comment that since we have not fixed an analogy, we do not prescribe the roles of X and Y here. A dissipator is called a *D-type dissipative element* in [3, Section 3.3], although only static dissipators are considered there.
- A *through-source*. Here the through variable T on the edge is externally prescribed.
- An *across-source*. Here the across variable A on the edge is externally prescribed.
- A *mixed-source*. Here two auxiliary variables v, λ are prescribed, and A and T are of the form $A = a(v, \lambda)$ and $T = t(v, \lambda)$ for functions $t, a : \mathbb{R} \to \mathbb{R}$.

The equations relating the across and through variables in the accumulator and dissipator elements are called *constitutive relationships*. The source terms shall play the role of either control terms or external signals. Observe that there are no constitutive relations for the source edges. It is this property that makes them somewhat different to the other edges.

Further, note that in both accumulator cases we have

$$\dot{E} = \frac{\partial E}{\partial x}\dot{x} = AT, \tag{3.1}$$

so that the product of the across and through variable indeed has the interpretation of power.

In the electrical context we have the following identifications: voltage is the across variable and current is the through variable. Moreover:

- A through-accumulator is an inductor with inductance L and the auxiliary variable x is *flux*.
- A across-accumulator is a capacitor with capacitance C and the auxiliary variable x is *charge*.
- A linear dissipator is a resistor with resistance R.
- A through-source is a current source.
- An across-source is a voltage source.

In the mechanical context we can either view velocity difference as the across variable and force as the through variable (this is called the *mobility analogy* and dates back to the work of Firestone [24] and Trent [25]) or the other way around (which is called the *impedance analogy*). Although each analogy has its own advantages and disadvantages, we prefer the former. One reason is that the graphs then look similar to the usual mechanical system diagrams typically drawn. Another reason is that the potential for the through variable then has the natural interpretation of velocity. Thus, in the translational mechanical context under the mobility analogy:

- A through-accumulator is a spring with spring constant $1/L$ and we have that x is *displacement*.
- An across-accumulator is a mass with mass C and we have that x is *momentum*. Here it would need to be assumed that all across accumulators in the system are connected to the same vertex (ground); otherwise the across-accumulator is an inerter [26].
- A linear dissipator is a dash-pot damper with damping coefficient R (as $T = RA$, that is, force is proportional to velocity difference with constant R).
- A through-source is a force source.
- An across-source is a velocity source.

As is well known, rotational mechanical, fluid and thermal systems may also be modelled by the control systems described in this section; see, for example, [6, Section 3] or [3, Section 3]. Finally, and as mentioned in Section 3.1, the mobility and impedance analogies are dual concepts, and so can be mapped between as necessary. This is particularly important when seeking to combine graphs from different energy domains.

3.4. Merging graphs

Many engineering systems, including renewable energy devices, are comprised of subsystems from distinct energy domains. To connect such subsystems requires energy converting elements, called transducers. When modelling control systems as linear graphs, transducers are two-port elements which map across/through variables in one domain (at one port) to either across/through variables or through/across variables in another (at the second port). A transducer is conventionally called a *transformer* when the analogy between variables is preserved, and a *gyrator* otherwise. Of course, a given transducer acts as either a transformer or gyrator depending on the analogies chosen in each energy domain.

Transducers are covered in depth in [3, Section 6] and [6, Chapters 5, 8 and 9], as well as throughout the text [5] for the coupling of electrical and mechanical systems. For brevity, we simply recall from [3, Section 6.2] that an ideal transducer is a *lossless* (or energy routing), *linear*, *static* two-port element, so has constitutive equation of the form

$$\begin{pmatrix} A_2 \\ T_2 \end{pmatrix} = G \begin{pmatrix} A_1 \\ T_1 \end{pmatrix}, \tag{3.2}$$

for across/through variable pairs (A_i, T_i), and where the 2×2 matrix G is of the form

$$G = \begin{pmatrix} -\kappa^{-1} & 0 \\ 0 & \kappa \end{pmatrix} \quad \text{or} \quad \begin{pmatrix} 0 & -\kappa^{-1} \\ \kappa & 0 \end{pmatrix} \qquad \kappa > 0,$$

for transformers and gyrators, respectively.

We give an example, based on [3, Figure 6.3(b), p. 172].

Example 3.2. A gear train (two connected cogwheels) is a transformer/gyrator which connects one rotational mechanical system to another. Let ω_k and T_k denote the angular velocity and torque of the kth cogwheel, respectively, for $k = 1, 2$. Suppose that the first and second cogwheel have n_1 and n_2 teeth, respectively, so that $\gamma := n_1/n_2 > 0$ denotes the gear ratio. Then the ideal gear equations are

$$\omega_2 = -\omega_1/\gamma \quad \text{and} \quad T_2 = \gamma T_1, \tag{3.3}$$

(note minus sign as cogwheels rotate in opposite directions) which may also expressed as a transformer/gyrator equation

$$\begin{pmatrix} \omega_2 \\ T_2 \end{pmatrix} = \begin{pmatrix} -\gamma^{-1} & 0 \\ 0 & \gamma \end{pmatrix} \begin{pmatrix} \omega_1 \\ T_1 \end{pmatrix} \qquad \text{or} \qquad \begin{pmatrix} 0 & -\gamma^{-1} \\ \gamma & 0 \end{pmatrix} \begin{pmatrix} T_1 \\ \omega_1 \end{pmatrix},$$

depending on the choice of across and through variables.

Presently, our aim is to use transducers to merge multiple subgraphs into a single graph, so that the energy-balance method is applicable. We do this as follows. We add an external edge to each graph to be merged, representing the through and across variables which enter the two ports of the transducer. The transducer equation (3.2) gives an algebraic relationship between the variables on the transducer edges. By appropriately rescaling the variables in one of the graphs, the variables on the two transformer edges become equal. The two graphs

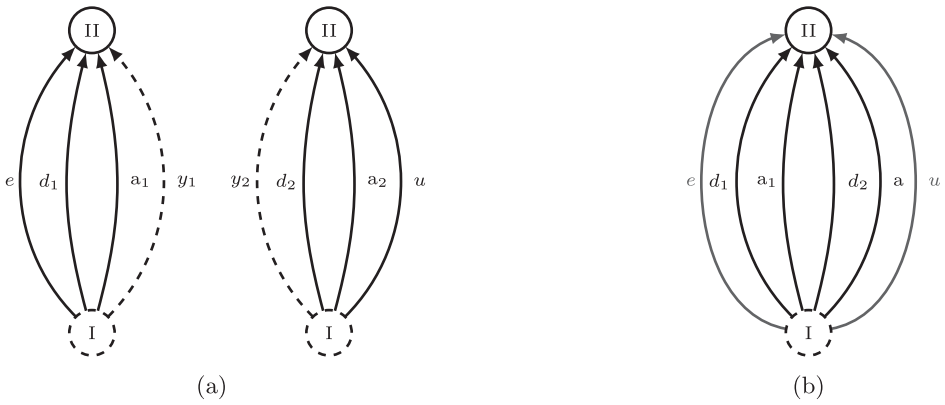

Fig. 3.2. Two rotating shafts connected by gear-train under mobility analogy. Dashed node is ground. (a) Separate graphs with dashed transformer edges (b) Merged graphs.

may then simply be connected at the nodes of the transformer edges, and these edges omitted. Importantly, when a transducer is a gyrator (so that an across variable is proportional to a through variable in a given energy domain), then the dual analogies need to be used between the two subgraphs, so as to obtain a consistent set of across/through edge functions for the whole graph.

Example 3.3. Consider two rotating shafts, labelled one and two, both with damping and inertia. The first and second shafts are subject to an external and control torque, respectively. The shafts are connected by an ideal gear train. Fig. 3.2(a) shows the graphs of both shafts (separately, before connection) under the mobility analogy, so that angular velocity differences are across variables and torques are through variables. The d and a edges denote dissipator (damping) and accumulator (inertia) elements. The dashed edges marked y_i are transformer edges.

Before merging the graphs, the through and across variables are denoted

$$\tilde{A}_1 = \begin{pmatrix} A_e \\ A_{d_1} \\ A_{\mathrm{a}_1} \end{pmatrix}, \quad \tilde{T}_1 = \begin{pmatrix} T_e \\ T_{d_1} \\ T_{\mathrm{a}_1} \end{pmatrix}, \quad \tilde{A}_2 = \begin{pmatrix} A_{d_2} \\ A_{\mathrm{a}_2} \\ A_u \end{pmatrix}, \quad \tilde{T}_2 = \begin{pmatrix} T_{d_1} \\ T_{\mathrm{a}_1} \\ T_u \end{pmatrix}.$$

We let (A_{y_i}, T_{y_i}) denote the across and through variables of the transformer edges. Observe that from the across equations we obtain

$$A_{y_i} = A_{d_i} = A_{\mathrm{a}_i} =: \omega_i, \quad i = 1, 2,$$

the angular velocity of the ith shaft, and the through equations give

$$T_x + T_{d_i} + T_{\mathrm{a}_i} + T_{y_i} = 0, \quad i = e, u,$$

the sum of the torques on the ith shaft.

In light of the gear Eqs. (3.3), by defining new across and through variables (A_2, T_2) as

$$A_2 := -\gamma \tilde{A}_2 \quad \text{and} \quad T_2 := \tilde{T}_2/\gamma,$$

it follows that $A_{y_2} = A_{y_1}$ and $T_{y_2} = T_{y_1}$. Therefore, the subgraphs may be merged by removing the transformer edges and connecting the two subgraphs at the transformer nodes. The merged graph is shown in Fig. 3.2(b). For simplicity, we have not changed the edge labels in the merged graph, but we comment that the constants in the elements of rescaled subgraphs also need to be rescaled.

We comment that transducers may be modelled to include energy storage or energy dissipation (such as a gear train having stiffness and damping) by including edges in the corresponding linear graph with accumulator or dissipator elements.

4. The energy-balance method for a two-source optimal control problem

Here we describe the energy-balance method for a two-source optimal control problem, which includes numerous renewable energy applications. In essence, we generalise the basic idea from Section 2 to control systems specified in terms of graphs and across/through edge functions from Section 3. The method is illustrated in a number of renewable energy settings across Sections 5–7.

We make the following assumptions:

- A control system (CS) is specified by a planar graph, with across edge function A and through edge function T, as in Section 3.
- There are precisely two sources in our graph. One of these is external, and we denote those edge variables by A_{e} and T_{e}. The other is the control, and we denote those edge variables by A_u and T_u. We assume that the sources have a vertex in common, chosen to be the ground vertex.
- There is a graph energy function E, which is equal to the sum of the energy functions E_k corresponding to each accumulator edge.
- An optimisation time interval $[t_0, t_1]$ is given, and the objective is to maximise

$$E(t_1) - E(t_0) + \int_{t_0}^{t_1} A_u T_u \, \mathrm{d}t \,, \tag{4.1}$$

subject to the control system (CS). Here $E(t_0)$ and $E(t_1)$ denote the energy in the system at the initial and final time, respectively; and $\int_{t_0}^{t_1} A_u T_u \, \mathrm{d}t$ equals the energy extracted from the system during the optimisation interval.

The *energy-balance equation* is

$$E(t_1) - E(t_0) + \int_{t_0}^{t_1} A_u T_u \, \mathrm{d}t = -\int_{t_0}^{t_1} A_{\mathrm{e}} T_{\mathrm{e}} \, \mathrm{d}t - \sum_{\text{dissipator}} \int_{t_0}^{t_1} A_k T_k \, \mathrm{d}t \,. \tag{4.2}$$

Eq. (4.2) generalises equality (2.5) from Section 2 to the general control system (CS). From a physical perspective the above equality corresponds to conservation of energy, taking into account sources and dissipation. A derivation of the energy-balance equation is given in Section 4.1. As with the problem studied in Section 2, maximising the left-hand side of (4.2), which equals the desired quantity to be maximised (4.1), is equivalent to maximising the right-hand side of (4.2) — our new performance objective.

In order to maximise the new performance objective we require a closed system of sufficiently many equations, and potentially additional variables which do not appear in the new performance objective, to determine all the variables which *do* appear. Equations may come from across/through equations from the graph, or constitutive relationships

on the edges. However, the fewer the variables and equations the better, as this leads to a simpler optimisation problem to solve. Indeed, the advantage of the method is that when enough equations are present, the variables which *do not* appear can be neglected from the new optimal control problem, reducing its size. Once the new optimisation problem is solved, the remaining variables are determined from the original constitutive relationships and the across/through equations.

Since the original problem corresponds to a control system specified by a graph — we employ a graph-theoretic approach to maximise the new performance objective. The problem is as follows. We are given a connected graph without self-loops, but probably with multiple edges. The new performance objective only includes the dissipator edges and the external source edge and, therefore, we seek a connected subgraph which includes these edges.

For which purpose, we give the original graph an *initial colouring*, in that we mark:

- the external edge and all dissipator edges green ;
- the control edge red, and ;
- the accumulator edges black.

(The choice of colours is of course arbitrary, what matters is that we partition these edges into three distinct groups.) By hypothesis, the control (red) and external (green) edges have a shared vertex; the ground. The objective is to partition the graph into two connected subgraphs which share the ground vertex and one other vertex (only) by marking each accumulator (black) edge as either red or green in such a way that the set of green edges is as small as possible. The smallest possible set of green edges comprises precisely the external edge and all the dissipator edges. However, in practice, some initially black edges may need to be marked green so that the resulting subgraph is connected. Therefore, an algorithm is required to colour each black (accumulator) edge in the initial colouring either green or red to meet the above objective.

We then view the green subgraph as a new control system, and maximise the new performance objective subject to this smaller control system. We call the process of using the energy-balance equation and graph-splitting procedure as outlined above to solve the original optimal control problem, *the energy-balance method*. Importantly, observe that the energy-balance method does not specify which optimisation technique is ultimately used for solving the subgraph optimisation problem. We view this as a strength as it means that the method is somewhat flexible and widely applicable. In certain cases, the new performance criterion is subject to no dynamic (state) constraints, and so becomes a classical optimisation problem, which may be solved by calculus methods such as gradient descent and its variations, or nonlinear programming, (see, for example [14,15]). When dynamic constraints are present, then a so-called trajectory optimisation problem remains. Our preference for solving such problems is the Pontryagin Principle (see, for instance [9–11]), but other methods are applicable here, as well as shooting or collocation direct methods.

The mathematical derivation in Section 4.1 shows that the above problem may always be solved — although with no *a priori* guarantee as to how many variables from the original problem may be omitted in the new performance objective. It is beyond the scope, and not the purpose, of the present work to exhaustively explore how to numerically compute such a partition of the original graph into two subgraphs, particularly for "large" graphs. For control systems specified by "small" graphs, it is possible simply to identify the desired subgraphs by inspection, as we do for the examples presented across Sections 5–7.

4.1. Mathematical derivations

Here we derive the energy-balance equation (4.2) and the graph-splitting procedure from the previous section.

In order to derive (4.2), we require Tellegen's Theorem [2]. In the present context, Tellegen's Theorem states that the across and through edge functions $A, T : \mathbb{R} \to \mathbb{R}^m$ are orthogonal (pointwise in time), meaning:

$$A^\top T = 0 \quad \text{or, in components,} \quad \sum_k A_k T_k = 0\,. \tag{4.3}$$

Integrating both sides of (4.3) from $t = t_0$ to $t = t_1$ yields that

$$\sum_k \int_{t_0}^{t_1} A_k T_k \,\mathrm{d}t = 0\,. \tag{4.4}$$

Splitting the sum in Eq. (4.4) into different edge types, (4.4) may be rewritten as

$$\begin{aligned} 0 &= \sum_k \int_{t_0}^{t_1} A_k T_k \,\mathrm{d}t \\ &= \sum_{\text{accumulator}} \int_{t_0}^{t_1} A_k T_k \,\mathrm{d}t + \int_{t_0}^{t_1} A_u T_u \,\mathrm{d}t + \int_{t_0}^{t_1} A_\mathrm{e} T_\mathrm{e} \,\mathrm{d}t + \sum_{\text{dissipator}} \int_{t_0}^{t_1} A_k T_k \,\mathrm{d}t\,, \end{aligned}$$

which we may rearrange to give

$$\sum_{\text{accumulator}} \int_{t_0}^{t_1} A_k T_k \,\mathrm{d}t + \int_{t_0}^{t_1} A_u T_u \,\mathrm{d}t = - \int_{t_0}^{t_1} A_\mathrm{e} T_\mathrm{e} \,\mathrm{d}t - \sum_{\text{dissipator}} \int_{t_0}^{t_1} A_k T_k \,\mathrm{d}t\,. \tag{4.5}$$

For each accumulator edge we have $\dot{E}_k = A_k T_k$ from (3.1), which we integrate between $t = t_0$ and $t = t_1$ to give

$$E_k(t_1) - E_k(t_0) = \int_{t_0}^{t_1} A_k T_k \,\mathrm{d}t.$$

Summing over all accumulator edges yields that

$$E(t_1) - E(t_0) = \sum_{\text{accumulator}} \int_{t_0}^{t_1} A_k T_k \,\mathrm{d}t\,. \tag{4.6}$$

Substituting (4.6) into (4.5) gives (4.2), as required.

We now derive the graph-splitting procedure. Suppose that we have a connected (green) subgraph comprising, at least, the external edge and the dissipator edges. The control edge is not included in this subgraph and, recall, the external edge and control edge share a vertex by hypothesis.

Assume that the subgraph has n_s vertices and m_s edges. We partition the across edge function A and through edge function T into

$$A = \begin{pmatrix} A_\mathrm{S} \\ A_\mathrm{C} \end{pmatrix} \quad \text{and} \quad T = \begin{pmatrix} T_\mathrm{S} \\ T_\mathrm{C} \end{pmatrix},$$

where A_S and T_S both have m_s components. Then we have m_s edge equations inherited from the original graph. To obtain across equations, we partition the face matrix $\mathcal{F}$ as follows

$$\mathcal{F} = \begin{pmatrix} \mathcal{F}_{11} & \mathcal{F}_{12} \\ \mathcal{F}_{21} & \mathcal{F}_{22} \end{pmatrix},$$

where the rows of $\mathcal{F}_{11}$ and $\mathcal{F}_{12}$ correspond to the green faces, and the columns correspond to the green and red edges, respectively. Since the green subgraph is connected by hypothesis, it follows that $\mathcal{F}_{11}$ is a compatibly-sized cycle submatrix[1] and there are no green faces with red edges, so that $\mathcal{F}_{12} = 0$. Therefore, we obtain the decomposition of the across equations

$$\mathcal{F}A = 0 = \begin{pmatrix} \mathcal{F}_{11} & \mathcal{F}_{12} \\ \mathcal{F}_{21} & \mathcal{F}_{22} \end{pmatrix} \begin{pmatrix} A_\mathrm{S} \\ A_\mathrm{C} \end{pmatrix} = \begin{pmatrix} \mathcal{F}_{11} & 0 \\ \mathcal{F}_{21} & \mathcal{F}_{22} \end{pmatrix} \begin{pmatrix} A_\mathrm{S} \\ A_\mathrm{C} \end{pmatrix}, \tag{4.7}$$

and, consequently,

$$\mathcal{F}_{11} A_\mathrm{S} = 0.$$

[1] In terms of the graph colouring described in Section 4, $\mathcal{F}_{11}$ corresponds to the "green faces", that is, the faces with green edges only. However, strictly, $\mathcal{F}_{11}$ is not a face matrix as it does not include a row for the unbounded face of the green subgraph.

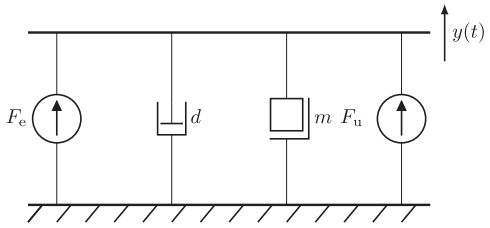

Fig. 4.1. Mechanical system diagram of the damped mass.

By Euler's formula, we obtain $m_s - n_s + 2 - 1 = m_s - n_s + 1$ independent across equations, as we have not included the unbounded face in the green subgraph.

Similarly, the through equations are

$$\mathcal{M}T = 0 = \begin{pmatrix} \mathcal{M}_{11} & \mathcal{M}_{12} \\ \mathcal{M}_{21} & \mathcal{M}_{22} \end{pmatrix} \begin{pmatrix} T_S \\ T_C \end{pmatrix},$$

but now $\mathcal{M}_{12} \neq 0$ in general and, in fact, we do not obtain through equations involving only through variables in T_S at vertices which are shared with the complement. Rather, if there are p shared vertices, then there are $n_s - p$ through equations for the green subgraph which involve only the through variables in T_S — these *are* inherited from the original graph.

Hence, the across/through equations yield so far

$$(m_s - n_s + 1) + (n_s - p) = m_s + 1 - p,$$

independent equations for the green subgraph. We need $m_s - 1$ through equations for T_S (involving only T_S) in addition to the edge equations, since we treat one edge variable as the independent variable for the new performance objective. This leads to $p = 2$. Note that since ground is one of the shared vertices by hypothesis, the graph-splitting procedure must identify exactly one additional shared vertex — doing so will generically give existence and uniqueness of solutions for the across function A_S and through function T_S.

4.2. The energy-balance method for a damped mass

We revisit the motivating damped mass example from Section 2, and now apply the energy-balance method presented in Section 4. To do so requires expressing the damped mass example as a linear graph, from Section 3. Whilst this level of abstraction may seem excessive for such a simple example, it becomes very useful for the more complicated situations considered later.

We present the mobility analogy, from which the impedance analogy may be treated by duality. In the mobility analogy, across variables are velocity differences and the through variables are forces. The damped mass as a mechanical system diagram is shown in Fig. 4.1. There are four "components", which will lead to a graph with four edges, corresponding to the mass, the damper, the external signal and the control signal.

Denote the across- and through-edge functions by A and T, respectively. In accordance with the splitting in Section 4.1, we order these as follows:

$$A := \begin{pmatrix} A_e \\ A_d \\ A_u \\ A_a \end{pmatrix} \quad \text{and} \quad T := \begin{pmatrix} T_e \\ T_d \\ T_u \\ T_a \end{pmatrix}.$$

The corresponding graph is given in Fig. 4.2(a), with its initial colouring. The nodes are labelled in the graph. By symmetry, which vertex is chosen as the ground is unimportant here. We label the external force, damper (dissipator), mass (accumulator) and control force edges as one to four, respectively. Therefore, the incidence matrix and face matrix are respectively given by

$$\mathcal{M} := \begin{pmatrix} 1 & 1 & 1 & 1 \\ -1 & -1 & -1 & -1 \end{pmatrix} \quad \text{and} \quad \mathcal{F} := \left(\begin{array}{cc|cc} 1 & -1 & 0 & 0 \\ 0 & 1 & -1 & 0 \\ 0 & 0 & 1 & -1 \\ \hline -1 & 0 & 0 & 1 \end{array}\right). \tag{4.8}$$

The faces are enumerated according to: left bounded face, middle bounded face, right bounded face, and unbounded face. The solid lines in $\mathcal{F}$ have been inserted to illustrate the decomposition of $\mathcal{F}$ as in (4.7).

The across equation $\mathcal{F}A = 0$ gives

$$A_e = A_d = A_a = A_u, \tag{4.9}$$

essentially stating that all the velocity differences act on the same single object (the mass).

The through equation $\mathcal{M}T = 0$ gives that

$$T_e + T_u + T_a + T_d = 0, \tag{4.10}$$

which, physically, is simply Newton's third law.

The constitutive relationships for the across-accumulator and dissipator are, respectively,

$$m\dot{A}_a = T_a \quad \text{and} \quad A_d = \frac{1}{d} T_d. \tag{4.11}$$

Therefore, with $T_e = -e$, $T_u = u$, and $A_a = y$, invoking (4.9), (4.10), and (4.11) gives that

$$m\dot{y} = m\dot{A}_a = T_a = -(T_e + T_u + T_d) = -e - u - d\,y,$$

which recovers (2.1).

At first sight, the six equations across (4.9), (4.10), and (4.11) may seem a cumbersome way of expressing the simple equation (2.1). However, the structured nature of those six equations, encoded by the graph in Fig. 4.2(a), has advantages which become more apparent in more complex situations. The right-hand side of the energy balance equation (4.2) is given by

$$-\int_{t_0}^{t_1} A_e T_e + A_d T_d \, \mathrm{d}t, \tag{4.12}$$

which is also equal to the right-hand side of (2.5).

Here the graph-splitting procedure is trivial. To partition the initial graph into two connected subgraphs (green edges and red edges) which share exactly two nodes, and where the green subgraph has as few edges as possible, it suffices to colour the black accumulator edge red, shown in Fig. 4.2(b). Both the subgraph (green edges) and its complement (red edges) have two edges, and share the only two vertices. For completeness, we record that the across edge function, through edge function, and the cycle matrix associated with green the subgraph are

$$A_S = \begin{pmatrix} A_e \\ A_d \end{pmatrix}, \quad T_S = \begin{pmatrix} T_e \\ T_d \end{pmatrix} \quad \text{and} \quad \mathcal{F}_S = \begin{pmatrix} 1 & -1 \end{pmatrix}, \tag{4.13}$$

respectively. Therefore, the across equation $\mathcal{F}_S A_S = 0$ yields

$$A_e = A_d.$$

We also retain the second constitutive equation from (4.11). However, as described in Section 4.1, the green subgraph inherits no through relationships from the original graph because the two (and so all the) vertices of the subgraph are shared with its complement. Finally, the external edge variable $T_e = -e$ is externally specified.

Thus, the energy-balance method reduces the current optimal control problem to maximising (4.12), in terms of the four unknowns, A_e, A_d, T_e and T_d. One of these variables is specified, and one shall play the role of the independent variable for the optimisation. This leaves two equations and two unknowns, which generically gives existence and uniqueness of solutions.

Fig. 4.2. Damped mass graph under mobility analogy. Yellow nodes are shared and the dashed node is ground. (a) Initial graph (b) Graph-splitting decomposition.

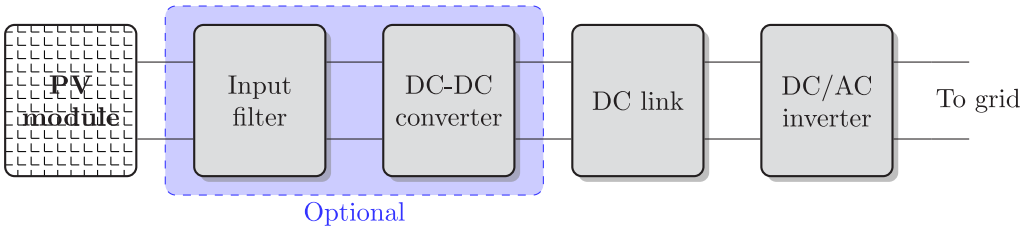

Fig. 5.1. Schematic of grid-connected PV system.

From here, the maximisation procedure is bespoke to the example under consideration. Presently, it is convenient to view A_e as the independent variable. In light of the across equation and constitutive relationship in (4.11), we seek to minimise

$$\int_{t_0}^{t_1} -A_e e + d A_e^2 \, \mathrm{d}t \, .$$

As before, this is achieving by pointwise minimising the integrand, to give $A_e = e/(2d) = -T_e/(2d)$, which determines the other variables A_d and T_d in the green subgraph. The remaining variables, those in the red subgraph, are now determined from (4.9), (4.10), and (4.11).

Of course, the above argumentation gives us the same as we obtained, in a seemingly easier way, in (2.7). However, as mentioned, the above graph-theoretic perspective provides a structured approach which generalises to much more complex situations.

5. Renewable energy application — solar

The remainder of the paper outlines the energy-balance method in the context of three different renewable energy technologies: solar, wind and wave. We begin with photovoltaic solar energy.

5.1. Background and existing works

A solar photovoltaic (PV) system essentially converts variable in time sunlight into electric power of a fixed frequency. The treatment of solar energy systems is now common in engineering textbooks, such as [27, Chapter 6], and recent reviews of PV systems include [28,29]. The basic component of a PV system is a PV cell, underpinned by the photovoltaic effect. PV cells are connected in series or parallel to form a PV module (also called a panel), collections of which are called a PV array or farm. PV modules or arrays generate a DC current which is transformed, via a PV inverter, and then may be connected to a utility grid. The generic structure of a grid-connected PV system is shown in [28, Figure 1] or [29, Fig. 14], from which Fig. 5.1 below is inspired.

We note that the input filter and DC/DC converter are marked as optional in Fig. 5.1. However, it is advantageous to individually control each solar module making up the array, and then this option is needed as highlighted in [29, p. 3128]. The objective is to maximise the total energy at the DC/AC interface. The subsystem comprising the DC link and the DC/AC converter is then left to deal with converting this to the desired frequency. We will concentrate on the subsystem comprising the PV module and the input filter. The DC/DC converter is typically modelled as an ideal transformer (see, for example [30, equation (31)]), and could easily be included in what follows.

PV systems are well-studied objects with a vast literature. The prevailing optimisation method is so-called Maximum Power Point Tracking (MPPT) with reviews including [31–35]. Roughly speaking, the Maximum Power Point is the voltage (load) point at which the power output of a PV module (described by the P–V characteristic) is maximised. MPPT then seeks to vary the voltage temporally so that the MPP is maintained. There are a range of MPPT algorithms, each with its advantages and disadvantages, such as those described in [33, Section 3], and we refer the reader to the references listed for more information. In Section 5.3 below we demonstrate how the MPPT problem naturally arises from the energy-balance method. By way of other recent related literature, the papers [36,37] explore, in different ways, the role of the DC–DC converter in optimal energy conversion.

5.2. A mathematical model

Details of the mathematical modelling of PV modules may be found in [38]. Here we make the further simplifying assumption that the PV module comprises a single PV cell — more complicated arrangements will be considered in later work. Furthermore, we do not consider the effects of temperature or partial shading, the latter of which is a current avenue of PV research; see, for example [39,40]. A simple equivalent circuit model for an ideal PV cell comprises an ideal current source in parallel with an ideal (or Shockley) diode. However, more realistic models for PV cells include losses within the cell are typically modelled by including shunt and series resistances; see, for example [38, Figure 4] or [27, Figure 5.14, p. 151]. Fig. 5.2 contains an electrical circuit model for a PV solar cell connected to a RLC filter, and the ideal PV cell is also outlined.

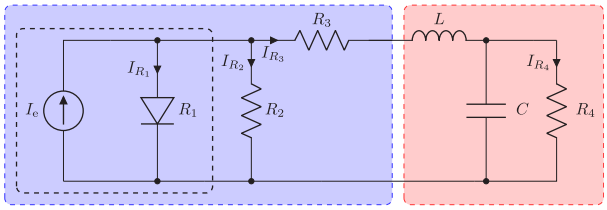

Fig. 5.2. Electrical circuit model for PV solar cell (blue box) and RLC filter (red box). The components inside the black box comprise the ideal PV cell.

With reference to Fig. 5.2, the current source is an external source, the diode is modelled as a nonlinear dissipator given by $V = R_1(I)$ where

$$R_1(I) := V_0 \ln\left(1 + \frac{I}{I_0}\right) \quad \text{or, equivalently,} \quad I = I_0 \exp\Big(\frac{V}{V_0} - 1\Big),$$

for positive constants V_0, I_0. Further, the shunt resistance R_2, series resistance R_3, and filter resistance R_4 are all modelled as linear dissipators. The control is the voltage across the capacitor; this is modelled as a voltage source, though for our purposes it does not really matter which of the three possible sources it is.

The corresponding linear graph is given in Fig. 5.3(a) with its initial colouring. Figs. 5.3(b) and 5.3(c) show the graph-splitting decomposition (with colourings) for the setting of an LC filter and RLC filter, respectively. As an electrical circuit example, the across and through variables in this example are voltage and current, respectively and, therefore, we use the notation $A_x = V_x$ and $T_y = I_y$ throughout.

In the following subsections we apply the energy-balance method to the PV solar cell (and RLC filter) models considered.

5.3. Maximum power point tracking for an ideal PV solar cell

For the ideal PV cell depicted in Fig. 5.2, elementary circuit modelling leads to the following relationship

$$I_u = I_e - I_0 \exp\Big(\frac{V_u}{V_0} - 1\Big), \tag{5.1}$$

so that the power output of the ideal solar PV cell is

$$P = I_u V_u = \Big(I_e - I_0 \exp\Big(\frac{V_u}{V_0} - 1\Big)\Big) V_u.$$

Here $I = I_u$ and $V = V_u$ are the load current and voltage, respectively. For fixed I_e, the graphs of these two equations are called the I–V characteristic and P–V characteristic of the ideal PV solar cell, respectively, and illustrative graphs are plotted in Fig. 5.4(a). It is readily seen that $P = P(V_u)$ has a unique maximum, and this point is called the Maximum Power Point (MPP) and denoted V_{MPP}. Since the P–V characteristic varies with time as the current source I_e varies, the MPP changes over time, that is, $V_{MPP} = V_{MPP}(t)$. MPPT methods essentially specify how to determine $V_{MPP}(t)$ temporally.

We show how the MPPT problem arises from the energy-balance method. Arguably, as with the damped mass considered in Sections 2 and 4.2, this level of abstraction may seem excessive for such a simple example, but we argue is extremely useful once more involved models are considered. The linear graph of the ideal PV cell is shown in Fig. 5.4(b), with the directions of the edges chosen to be consistent with the signs used in (5.1). In this problem there are six variables

$$I_e,\ V_e,\ I_{R_1},\ V_{R_1},\ V_u,\ I_u, \tag{5.2}$$

(where I_{R_1}, V_{R_1} are the current voltage pair for the diode), a single through equation

$$I_u = I_e - I_{R_1} \quad \text{(from either node)},$$

two across equations

$$V_{R_1} = -V_e \quad \text{and} \quad V_{R_1} = V_u, \quad \text{(from the e–}R_1\text{ and }R_1\text{–}u\text{ faces)}, \tag{5.3}$$

and the constitutive relationship

$$V_{R_1} = R_1(I_{R_1}) = V_0 \ln\left(1 + \frac{I_{R_1}}{I_0}\right) \quad \text{or, equivalently,} \quad I_{R_1} = I_0\Big(\exp\Big(\frac{V_{R_1}}{V_0}\Big) - 1\Big). \tag{5.4}$$

Presently, the energy-balance equation (4.2) reads

$$\int_{t_0}^{t_1} I_u V_u \,\mathrm{d}t = -\int_{t_0}^{t_1} I_e V_e + I_{R_1} V_{R_1} \,\mathrm{d}t, \tag{5.5}$$

as there are no energy storage elements (accumulators) here. The desired aim of maximising the left-hand side of (5.5) is equivalent to maximising the right-hand side, which depends on four variables and is subject to no dynamic constraints. Hence, maximisation is achieved by pointwise maximisation (in time) of the integrand. Of the four variables, one is externally specified and one shall play the role of the independent variable used for the optimisation. Therefore, we require two equations relating these four variables. Whilst it is clear in this simple example which equations these are, with reference to the graph-splitting procedure, observe that the green subgraph inherits no through relationships from the original graph because the two (and so all the) nodes of the subgraph are shared with its complement. However, the first across equation in (5.3) and the constitutive relationship (5.4) are inherited by the green subgraph, yielding the two required equations. To maximise the integrand on the right-hand side of (5.5), we first rewrite it in terms of the variable V_{R_1} and external source I_e as

$$V_{R_1}\Big(I_e - I_0\Big(\exp\Big(\frac{V_{R_1}}{V_0}\Big) - 1\Big)\Big).$$

Maximising the above function gives the MPP, as expected.

5.4. Solar cell with a LC filter

Here we consider the arrangement in Fig. 5.3(b). The right-hand side of the energy-balance equation (4.2) equals

$$-\int_{t_0}^{t_1} V_e I_e \,\mathrm{d}t - \sum_{\text{dissipator}} \int_{t_0}^{t_1} V_k I_k \,\mathrm{d}t = -\int_{t_0}^{t_1} V_e I_e + V_{R_1} I_{R_1} + V_{R_2} I_{R_2} + V_{R_3} I_{R_3} \,\mathrm{d}t.$$

Hence, the objective is to minimise

$$\int_{t_0}^{t_1} V_e I_e + V_{R_1} I_{R_1} + V_{R_2} I_{R_2} + V_{R_3} I_{R_3} \,\mathrm{d}t,$$

subject to the algebraic constitutive relationships

$$\left.\begin{aligned} &V_{R_1} = V_0 \ln\left(1 + \frac{I_{R_1}}{I_0}\right), \qquad V_{R_2} = R_2 I_{R_2}, \\ &V_{R_3} = R_3 I_{R_3}, \end{aligned}\right\} \quad \text{(from the green dissipator edges)},$$

the through equation

$$I_{R_1} + I_{R_2} + I_e = I_{R_3} \quad \text{(from the green node (III))},$$

the across equations

$$V_e = V_{R_1} = V_{R_2} \quad \text{(from the } R_1\text{–e and } R_2\text{–e faces)},$$

and we recall that I_e (from the green edge e) is externally given. The optimisation involves eight variables, one of which is externally specified and one of which shall play the role of the independent variable in the optimisation. This leaves six unknowns and six equations above, which generically gives existence and uniqueness of solutions.

Since the optimal control problem associated with the energy-balance method only involves algebraic equations, it can be solved by pointwise minimisation of the integrand. It is convenient to choose I_{R_1} as the independent variable. We use the algebraic equations to write the integrand in terms of I_{R_1} and the given I_e as

$$\left(\frac{R_2 + R_3}{R_2} V_0 \ln\left(1 + \frac{I_{R_1}}{I_0}\right) + R_3 I_e + R_3 I_{R_1}\right)\left(\frac{1}{R_2} V_0 \ln\left(1 + \frac{I_{R_1}}{I_0}\right) + I_e + I_{R_1}\right).$$

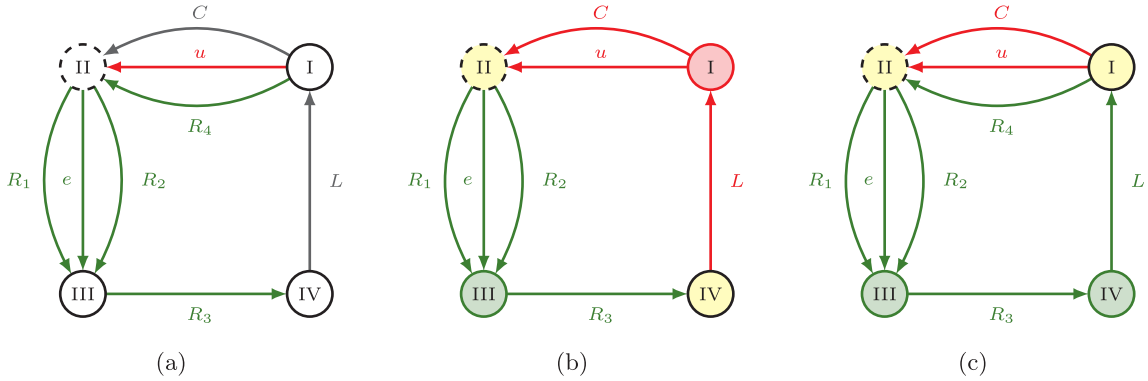

Fig. 5.3. PV RLC circuit model as graph. Yellow nodes are shared and the dashed node is ground. (a) Initial colouring of graph with RLC filter (b) Subgraph and its complement for the LC filter (c) Subgraph and its complement for the RLC filter.

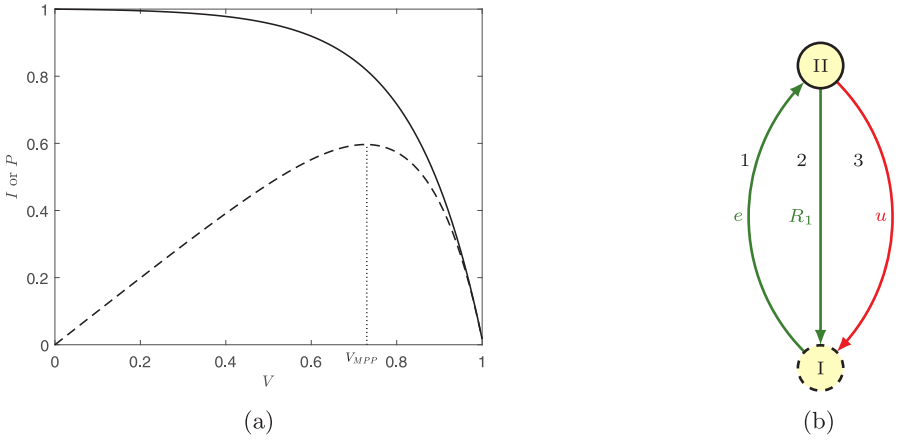

Fig. 5.4. (a) I–V characteristic (solid) and P–V characteristic (dashed) of the ideal PV solar cell. The maximum power point (MPP) is shown. (b) Linear graph for the ideal PV solar cell. The subgraph and its complement are shown. Yellow nodes are shared and the dashed node is ground.

From setting the derivative of the integrand with respect to I_{R_1} equal to zero, we obtain

$$\Big(\frac{R_2+R_3}{R_2}V_0\ln\Big(1+\frac{I_{R_1}}{I_0}\Big)+R_3I_e+R_3I_{R_1}\Big)\Big(\frac{V_0}{R_2(I_0+I_{R_1})}+1\Big)$$
$$\Big(\frac{(R_2+R_3)V_0}{R_2(I_0+I_{R_1})}+R_3\Big)\Big(\frac{1}{R_2}V_0\ln\Big(1+\frac{I_{R_1}}{I_0}\Big)+I_e+I_{R_1}\Big)=0, \tag{5.6}$$

as a necessary condition for an optimum. Developing equation (5.6) further analytically seems intractable, and numerical solutions will be required. Note that, including (5.6) we now have seven equations in seven variables.

Once the optimal control problem for the green subgraph is solved, we use the remaining equations to determine the remaining variables. These equations are

$$L\dot{I}_L=V_L,\qquad C\dot{A}_C=I_C,\qquad V_{R_4}=R_4I_{R_4},\qquad I_{R_3}=I_L,\qquad V_u=V_{R_4}=V_C,$$

and

$$V_u+V_e+V_{R_3}+V_L=0,\qquad I_L=I_{R_4}+I_C+I_u.$$

5.5. Solar cell with a RLC filter

Here we consider the arrangement in Fig. 5.3(c). The right-hand side of the energy-balance equation (4.2) equals

$$-\int_{t_0}^{t_1}V_eI_e\,\mathrm{d}t-\sum_{\text{dissipator}}\int_{t_0}^{t_1}V_kI_k\,\mathrm{d}t$$
$$=-\int_{t_0}^{t_1}V_eI_e+V_{R_1}I_{R_1}+V_{R_2}I_{R_2}+V_{R_3}I_{R_3}+V_{R_4}I_{R_4}\,\mathrm{d}t.$$

Hence, we seek to minimise

$$\int_{t_0}^{t_1}V_eI_e+V_{R_1}I_{R_1}+V_{R_2}I_{R_2}+V_{R_3}I_{R_3}+V_{R_4}I_{R_4}\,\mathrm{d}t,$$

subject to the algebraic and differential constitutive relationships

$$\left.\begin{aligned}&V_{R_1}=V_0\ln\Big(1+\frac{I_{R_1}}{I_0}\Big),\quad && V_{R_2}=R_2I_{R_2}\\ &V_{R_3}=R_3I_{R_3} && V_{R_4}=R_4I_{R_4}\\ &L\dot{I}_L=V_L,\end{aligned}\right\}\quad\text{(from the green edges)},$$

the through equations

$$I_{R_1}+I_{R_2}+I_e=I_{R_3},\qquad I_{R_3}=I_L\quad\text{(from the green vertices (III) and (IV))},$$

and the across equations

$$V_e=V_{R_1}=V_{R_2},\qquad V_{R_4}+V_e+V_{R_3}+V_L=0\quad\text{(from the three green faces)}.$$

We recall that I_e is externally given, and one variable shall play the role of an independent variable for the optimisation. Consequently, we are left with ten unknowns and ten equations, which generically gives existence and uniqueness of solutions. By way of commentary, observe from Fig. 5.3(c) that in order to construct a connected subgraph which contains all the dissipator edges, particularly R_4, the accumulator edge with across variable V_L and through variable I_L has been included. These variables do not appear in the right-hand side of (4.2), but are required to ensure that enough equations are specified to (uniquely) determine the variables which do appear.

In contrast to the situation of the LC filter, the current optimal control problem is subject to a single dynamic equation, $L\dot{I}_L=V_L$.

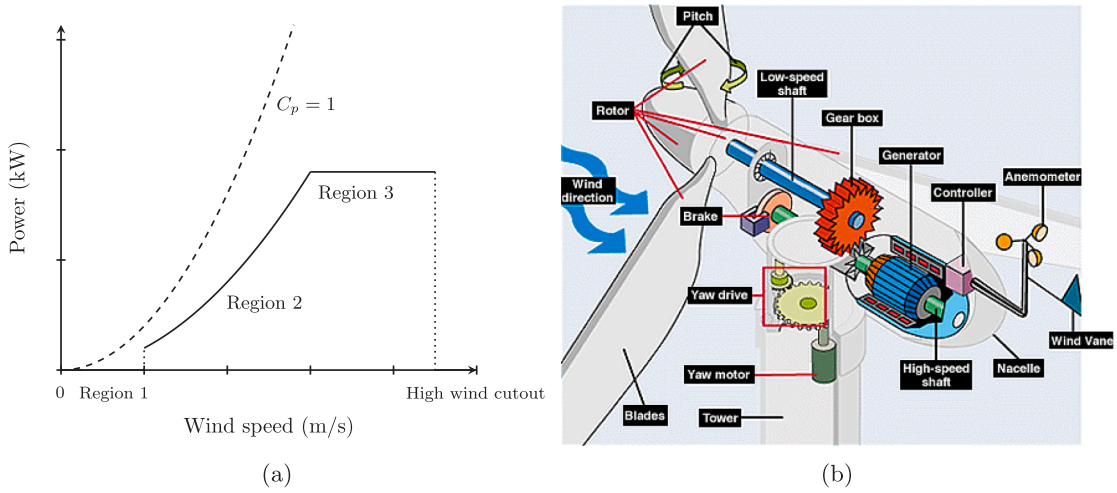

Fig. 6.1. Wind turbine figures (a) Schematic graph of regions of operation. Dashed line is wind power and solid line is turbine power. Figure is based on [44, Figure 3]. (b) Diagram of horizontal axis wind turbine. Figure is in the public domain and is courtesy of U.S. Department of Energy.

Therefore, solving this optimal control problem requires the Pontryagin Principle, or some other optimal control method. We note that the natural choice for control variable is I_{R_1} and that the Hamiltonian is non-affine in this new control variable, which is advantageous from a numerical perspective.

Once the optimal control problem for the subgraph is solved, we use the remaining equations to determine the remaining variables, namely, V_C, I_C, V_u and I_u. These equations are

$$C\dot{A}_C = I_C, \qquad V_u = V_{R_4} = V_C, \qquad I_L = I_{R_4} + I_C + I_u.$$

6. Renewable energy application — wind

6.1. Background and existing works

A wind turbine system essentially converts variable in time aerodynamic power into electric power of a fixed frequency. Nowadays wind energy is commonly used globally. It is both a growing source of renewable energy and, in 2021, generated more energy than all other non-hydro renewable sources combined [41]. The mathematical modelling of wind turbines is addressed in the works [42,43], and reviews of wind energy technology and control include [44–47]. We refer the reader to these papers and, for example, the texts [48] or [27, Chapter 2] for thorough treatments. Research into wind energy technology is multi-faceted, with two current lines of enquiry including improving the monitoring and maintenance of wind turbine blades [49,50], and vibration reduction control of wind turbine towers [51].

The operation of a wind turbine is as in Fig. 6.1(a): both at low wind speed and at very high wind speed the blades do not move; in "region 3" the power is held constant; it is "region 2" which is of interest to us — this is where the turbine operates in an energy capture maximising fashion.

The main mechanical components of a horizontal-axis wind turbine are illustrated in Fig. 6.1(b). Attached to the rotor is the low-speed shaft which is connected via a gear to the high-speed shaft. The high-speed shaft is connected to a generator. The control variable is the torque applied to the high-speed shaft. For simplicity, we assume that the pitch is constant throughout, so that we ignore controlling the pitch via the yaw motor. A wind turbine also contains an electrical subsystem (see, for instance [52, Figure 4]), the role of which is to convert the mechanical energy into electrical energy of a desired frequency. Presently, the objective is to maximise the energy at the mechanical–electrical interface. We assume that the low-speed shaft, high-speed shaft and gear all have damping and inertia, and, further, that we can control the electromechanical torque directly. In the model in [52] this is indirectly controlled through the electrical subsystem; this can be incorporated easily enough into the present framework.

6.2. A mathematical model

For a graph-theoretic model of the mechanical subsystem of a wind turbine, we choose (scaled) angular velocity differences as the across variables and (scaled) torques as the through variables. Specifically, we scale the across/through variables for the high-speed shaft as in Example 3.3 to obtain a single linear graph. Recall that the coefficients in the edge equations related to the high-speed shaft are then scaled by the square of the gear ratio compared to what they would have been had we taken velocity and torque as the variables. Since all the elements are linear, we simply relabel the relevant coefficients.

The external source is a mixed source which, recall, must be specified in terms of two auxiliary/external variables. The across variable A_e is the angular velocity of the blades and the through variable T_e is the aerodynamic torque acting on the blades which are related by

$$T_e = -C_q(\lambda)\frac{\rho a r}{2}v^2, \qquad \lambda = \frac{A_e r}{v}, \qquad C_q(\lambda) := \frac{C_p(\lambda)}{\lambda}, \tag{6.1}$$

where v is the wind speed, λ is the tip-speed ratio, ρ is the air density, r is the radius of the rotor blades, and $a = \pi r^2$ is the area swept by the turbine blades. The function C_p is referred to as the *power coefficient*, it takes positive values and has a unique maximum. It is determined experimentally — a sample curve is contained in [44, Figure 3]. The variables A_e and T_e are uniquely determined by v and λ via (6.1), and we view these latter two as the two independent variables in the mixed source.

The three energy-dissipating elements are all modelled as linear resistors. The control variable is the torque applied to the high-speed shaft, which is a through source. This gives the graph in Figs. 6.2(c) and a description of the edges appears in Table 6.1.

If, in fact, it is assumed that there is no stiffness and damping in the gear (so that $L = 0$ and $R_3 = 0$), then the above is what is referred to as a *one-inertia model* of a gear; see, for example [44, Equation (7)]. This is the situation considered in Example 3.3. When there is stiffness in the gear, and possibly damping, then the above model is referred to as a *two-inertia model* of a gear; see, for example [53] and [30, Equation (16)] for multiple-inertia models.

From a linear graph modelling perspective, the difference between the one- and two-inertia models is that the L and R_3 edges are absent in the former. The initial graphs and graph-splitting decompositions of the one- and two-inertia models described are shown in Fig. 6.2. In the two-inertia model the accumulator edges L and C_3 are required to

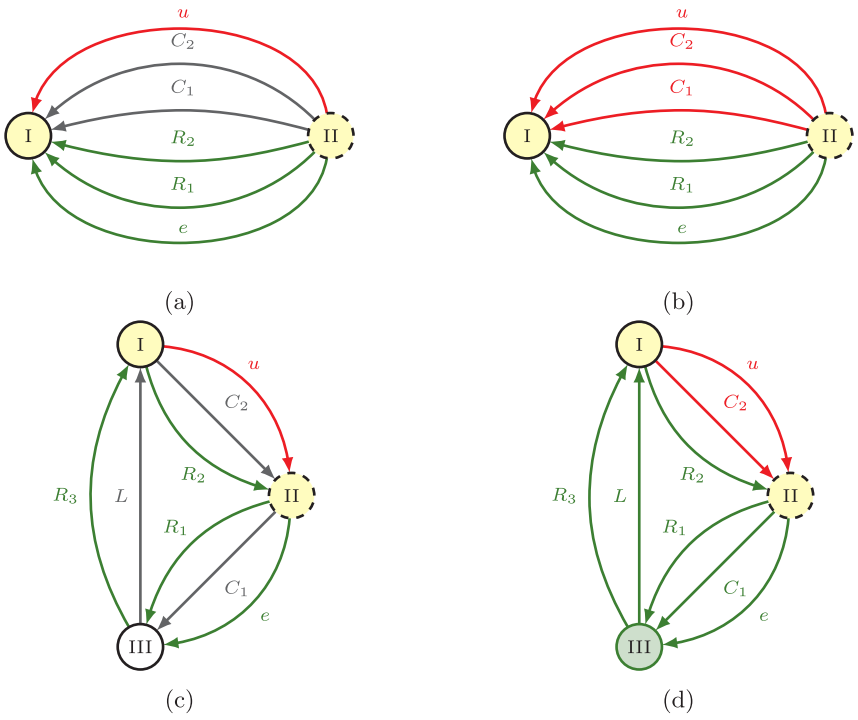

Fig. 6.2. Wind turbine models as linear graphs. Yellow nodes are shared and the dashed node is ground. (a) and (c) Initial graphs for one- and two-inertia models, respectively. (b) and (d) Graph-splitting decompositions for one- and two-inertia models, respectively.

Table 6.1
Edges for linear graph of wind turbine in Fig. 6.2(c).

Edge label	Description	Element type
e	Angular velocity/torque of rotor blades	Mixed source
R_1	Low-speed shaft damping	Linear dissipator
R_2	High-speed shaft damping	Linear dissipator
R_3	Gear damping	Linear dissipator
C_1	Low-speed shaft inertia	Across accumulator
C_2	High-speed shaft inertia	Across accumulator
L	Gear stiffness	Through accumulator
u	Control torque applied to high-speed shaft	Through source

belong to the green subgraph rather than the red subgraph, as otherwise the green and red subgraphs would share three nodes.

In the following subsections we apply the energy-balance method for the two wind turbine models considered.

6.3. One-inertia wind turbine model

Here we consider the arrangement in Fig. 6.2(a). At face value, we have an optimal control problem in the 12 variables

$$A_{\mathrm{e}},\ T_{\mathrm{e}},\ A_u,\ T_u,\ A_{R_1},\ T_{R_1},\ A_{R_2},\ T_{R_2},\ A_{C_1},\ T_{C_1},\ A_{C_2},\ T_{C_2}\,. \tag{6.2}$$

However, here the right-hand side of the energy-balance equation (4.2) equals

$$-\int_{t_0}^{t_1} A_{\mathrm{e}}T_{\mathrm{e}}\,\mathrm{d}t - \sum_{\text{dissipator}}\int_{t_0}^{t_1} A_kT_k\,\mathrm{d}t = -\int_{t_0}^{t_1} A_{\mathrm{e}}T_{\mathrm{e}} + A_{R_1}T_{R_1} + A_{R_2}T_{R_2}\,\mathrm{d}t.$$

Therefore, the objective is to minimise

$$\int_{t_0}^{t_1} A_{\mathrm{e}}T_{\mathrm{e}} + A_{R_1}T_{R_1} + A_{R_2}T_{R_2}\,\mathrm{d}t\,, \tag{6.3}$$

subject to the algebraic constitutive relationships

$$A_{R_1} = R_1T_{R_1}\,, \qquad A_{R_2} = R_2T_{R_2} \quad \text{(from the two green dissipator edges)},$$

the across equations

$$A_{R_1} = A_{\mathrm{e}} = A_{R_2}, \quad \text{(from two green faces)},$$

and we recall that the external edge variables A_{e} and T_{e} are determined in (6.1) by the external variable, the wind speed v, and the auxiliary variable, the tip-speed ratio λ. The green subgraph inherits no through relationships from the original graph because the two (and so all the) nodes of the subgraph are shared with its complement. As usual, one variable in the integrand (6.3) will play the role of the independent variable for the optimisation.

Thus, the energy-balance method reduces the original optimal control problem to another in terms of six variables

$$v, \lambda, A_{R_1}, T_{R_1}, A_{R_2}, T_{R_2}$$

related by four equations, and of which the first is externally given and one variable is chosen to be independent. Thus, existence and uniqueness of solutions is generically guaranteed.

Since the optimal control problem obtained by the energy-balance method only involves algebraic equations, it can be solved by pointwise minimisation of the integrand. For which purpose, we first rewrite the integrand in terms of A_{e}. We use the algebraic equations to write the integrand in terms of A_{e} as

$$A_{\mathrm{e}}T_{\mathrm{e}} + A_{R_1}T_{R_1} + A_{R_2}T_{R_2} = A_{\mathrm{e}}T_{\mathrm{e}} + A_{\mathrm{e}}^2\Big(\frac{1}{R_1} + \frac{1}{R_2}\Big).$$

It is now convenient to switch to the tip-speed ratio λ as independent variable. Invoking (6.1), the integrand is then equal to

$$-C_p(\lambda)\frac{\rho a}{2}v^3 + \frac{\lambda^2v^2}{r^2}\Big(\frac{1}{R_1} + \frac{1}{R_2}\Big), \tag{6.4}$$

which we seek to minimise as a function of λ. In the absence of an analytic expression for C_p, this needs to be done numerically, and gives rise to some $\lambda_\dagger > 0$ such that

$$A_{\mathrm{e}}^\dagger(t) = \frac{\lambda_\dagger}{r}v(t),$$

that is, the optimal speed of the low-speed shaft is proportional to the wind speed with proportionality constant $\lambda_\dagger/r$.

However, if the dissipators are absent, then (6.4) simplifies to $-C_p(\lambda)\rho a v^3/2$, and minimising this is equivalent to maximising the power coefficient C_p. In particular, we recover the same energy maximising control as the Standard Variable-Speed Control Law in [44, pp.73–74], although here from the energy-balance method. Let λ_* denote the unique point where C_p is maximised. Then, still in the absence of dissipators,

$$A_{\mathrm{e}}^*(t) = \frac{\lambda_*}{r} v(t),$$

It follows from the shape of C_p that $\lambda_\dagger < \lambda_*$, and so the optimal speed of the low-speed shaft is still proportional to the wind speed, but with a larger proportionality constant than in the presence of dissipators.

Once the optimal control problem for the green subgraph is solved, we use the remaining six equations to determine the remaining six variables. These equations are

$$C_1\dot{A}_{C_1} = T_{C_1}, \qquad C_2\dot{A}_{C_2} = T_{C_2},$$
$$A_{C_1} = A_{C_2} = A_u = A_{\mathrm{e}}, \qquad T_{\mathrm{e}} + T_{C_1} + T_{R_1} = -(T_u + T_{C_2} + T_{R_2}).$$

6.4. Two-inertia wind turbine model

Here we consider the arrangement in Fig. 6.2(c). We have an optimal control problem in 16 variables — 12 from (6.2), and

$$A_{R_3},\ T_{R_3},\ A_L,\ T_L. \tag{6.5}$$

Here, the right-hand side of the energy-balance equation (4.2) equals

$$-\int_{t_0}^{t_1} A_{\mathrm{e}}T_{\mathrm{e}}\,\mathrm{d}t - \sum_{\text{dissipator}} \int_{t_0}^{t_1} A_kT_k\,\mathrm{d}t = -\int_{t_0}^{t_1} A_{\mathrm{e}}T_{\mathrm{e}} + A_{R_1}T_{R_1} + A_{R_2}T_{R_2} + A_{R_3}T_{R_3}\,\mathrm{d}t.$$

Therefore, the objective is to minimise

$$\int_{t_0}^{t_1} A_{\mathrm{e}}T_{\mathrm{e}} + A_{R_1}T_{R_1} + A_{R_2}T_{R_2} + A_{R_3}T_{R_3}\,\mathrm{d}t,$$

subject to the constitutive relationships

$$\left.\begin{aligned} A_{R_1} = R_1T_{R_1},\ A_{R_2} = R_2T_{R_2},\ A_{R_3} = R_3T_{R_3},\\ C_1\dot{A}_{C_1} = T_{C_1},\ L\dot{T}_L = A_L, \end{aligned}\right\}$$
(from the green dissipator/accumulator edges),

the through equation

$$T_{R_1} + T_{C_1} + T_{\mathrm{e}} = T_{R_3} + T_L \qquad \text{(from the single green vertex)},$$

and the across equations

$$\left.\begin{aligned} A_{\mathrm{e}} = A_{R_1} = A_{C_1}, \quad A_{R_3} = A_L,\\ A_{R_1} + A_{R_2} + A_{R_3} = 0, \end{aligned}\right\} \quad \text{(from the four green faces)},$$

and we recall that T_{e} and A_{e} are determined by v and λ via (6.1).

The optimal control problem obtained by the energy-balance method has two state variables, A_{C_1} and T_L, and can be solved using the Pontryagin Principle, or some other optimal control method. We note that the natural choice for the control variable is A_L. We can write the integrand in terms of this new control and the state as

$$-C_p\left(\frac{A_{C_1}r}{v}\right)\frac{\rho a v^3}{2} + \frac{A_{C_1}^2}{R_1} + \frac{(A_{C_1}+A_L)^2}{R_2} + \frac{A_L^2}{R_3}.$$

The differential equation constraints are

$$C_1\dot{A}_{C_1} = \frac{A_L}{R_3} + T_L - \frac{A_{C_1}}{R_1} + C_q\left(\frac{A_{C_1}r}{v}\right)\frac{\rho a r v^2}{2}, \qquad L\dot{T}_L = A_L.$$

Once the optimal control problem for the green subgraph is solved, we use the remaining four equations to determine the remaining four variables (A_{C_2}, T_{C_2}, A_u and T_u). These equations are

$$C_2\dot{A}_{C_2} = T_{C_2}, \qquad A_u = A_{R_2} = A_{C_2}, \qquad T_{\mathrm{e}} + T_{C_1} + T_{R_1} = T_u + T_{C_2} + T_{R_2}.$$

7. Renewable energy application — wave

7.1. Background and existing works

There are a multitude of wave energy converter (WEC) technologies, including point absorber, attenuator, terminator and overtopping (offshore) devices, as well as oscillating wave surge converters (typically nearshore) and oscillating water column (typically shoreline). These technologies are reviewed across [8,54–56], with the works [57–59] focussing on oscillating water columns, point absorbers, and power take-off systems, respectively. The control of WECs has garnered much interest, and reviews specifically of the control of WECs include [60–62]. Recent perspectives and a nice summary of the research 'landscape', appear in [8]. Arguably, the established text in the field is that of Falnes [17], with more recent text [63]. There is broad consensus from researchers in the field that there is vast, as yet mostly untapped, potential for wave energy globally yet, despite now considerable research over the past three decades, *"wave energy has not yet reached commercial viability"* [8, Abstract] and *"In comparison to other sources of renewable energy, wave energy is still too expensive"*. [56, Section 4]. To illustrate the range of ideas being considered, the paper [64] reported nearly 150 WECs in development in 2013.

Roughly speaking, the hydrodynamic modelling and subsequent control of wave energy converters under linear dynamics is well understood [65] (even if still not straightforward to implement practically), but wave energy particularly is an area where consideration of nonlinear effects is important, as discussed in [66]. We reemphasise that the energy-balance method is applicable in a variety of nonlinear settings. In addition to the above researches, other current lines of enquiry include: real time prediction of incoming wave forces [67]; the exploration of hybrid wave-wind renewable energy technologies [68], seeking to leverage existing infrastructure of offshore wind, and; the grid integration challenges associated with renewable wave energy [69].

7.2. A mathematical model

The energy-balance method has already been illustrated in the context of wave energy, as the damped mass considered in Section 2 is a highly simplistic model of a point absorber moving in the heave direction only. As mentioned there, the known formulae in (2.7) from the WEC literature are almost trivially obtained by the energy-balance method, and do not make assumptions on the nature of the excitation force e.

As a different example, here we apply the energy-balance method to a simplified WEC model comprising a hull and a gyroscope. The hull oscillates owing to a force exerted by waves. The hull is also affected by a radiation system — the force on the hull caused by the radiated waves from the hull. The resulting energy is transferred to a gyroscope from where it is converted into electrical energy. For simplicity, the parts of the system downstream from the gyroscope are ignored, but those could be easily incorporated into the present framework. This device is called an *Inertial Sea Wave Energy Converter* (ISWEC). We refer the reader to [70], and the references therein, for information on the history and academic research on ISWECs. We comment that the same model has been studied for gyrostabilisation of ships; see, for example [71].

We first write down the equations of motion before considering a linear graph.

Denote the angular velocity of the hull by ω_{h} and its moment of inertia by J_{h}. The hull experiences a stiffness torque $F_{k_{\mathrm{h}}}$ and nonlinear damping torque $F_{d_{\mathrm{h}}}$ which satisfy

$$\dot{F}_{k_{\mathrm{h}}} = k_{\mathrm{h}}\omega_{\mathrm{h}} \quad \text{and} \quad F_{d_{\mathrm{h}}} = d_{\mathrm{h}}|\omega_{\mathrm{h}}|\omega_{\mathrm{h}}.$$

Here k_{h} and d_{h} are positive constants.

There is a torque arising from the radiation system given by C_Rz, where z is the state of the radiation system which is modelled by a

Table 7.1
Edges for linear graph of hull system in Fig. 7.1(a).

Edge label	Description	Element type
e	Torque from the incoming waves	Through source
R_1	Hull damping	Nonlinear dissipator
R_2	Damping from radiation system	Dynamic dissipator
C_1	Hull inertia	Across accumulator
L_1	Hull stiffness	Though accumulator
Gyro	Torque imposed on the hull by the gyroscope	One-port of transducer

Table 7.2
Edges for linear graph of gyroscope system in Fig. 7.1(b).

Edge label	Description	Element type
u	Control torque	Across source
R_3	Gyroscope damping	Linear dissipator
L_2	Gyroscope inertia	Through accumulator
C_2	Gyroscope stiffness	Across accumulator
Hull	Torque imposed on the gyroscope by the hull	One-port of transducer

linear, finite-dimensional state space control system

$$\dot{z} = A_R z + B_R \omega_{\mathrm{h}},$$

whose transfer function (from ω_{h} to $C_R z$) is assumed to be positive real. Denoting the angular position of the gyroscope by y_{g} and its angular velocity by ω_{g}, which are related by the differential equation $\dot{y}_{\mathrm{g}} = \omega_{\mathrm{g}}$, there is a torque imposed on the hull given by $\eta\omega_{\mathrm{g}}\cos(y_{\mathrm{g}})$ for some positive constant η. Finally, the incoming waves impose a torque F_{e} on the hull. Therefore, the dynamics of the hull are given by

$$J_{\mathrm{h}}\dot{\omega}_{\mathrm{h}} + d_{\mathrm{h}}|\omega_{\mathrm{h}}|\omega_{\mathrm{h}} + F_{k_{\mathrm{h}}} - \eta\omega_{\mathrm{g}}\cos(y_{\mathrm{g}}) + C_R z + F_{\mathrm{e}} = 0, \qquad \dot{F}_{k_{\mathrm{h}}} = k_{\mathrm{h}}\omega_{\mathrm{h}}. \quad (7.1)$$

The gyroscope has moment of inertia J_{g}, stiffness satisfying $\dot{F}_{k_{\mathrm{g}}} = k_{\mathrm{g}}\omega_{\mathrm{g}}\cos(y_{\mathrm{g}})$ (consistent with $F_{k_{\mathrm{g}}} = k_{\mathrm{g}}\sin(y_{\mathrm{g}})$), damping $d_{\mathrm{g}}\omega_{\mathrm{g}}$, a torque imposed by the hull of $-\eta\omega_{\mathrm{h}}\cos(y_{\mathrm{g}})$ and a control torque F_u. Therefore, the dynamics of the gyroscope are given by

$$J_{\mathrm{g}}\dot{\omega}_{\mathrm{g}} + d_{\mathrm{g}}\omega_{\mathrm{g}} + F_{k_{\mathrm{g}}} + \eta\omega_{\mathrm{h}}\cos(y_{\mathrm{g}}) + F_u = 0, \qquad \dot{F}_{k_{\mathrm{g}}} = k_{\mathrm{g}}\omega_{\mathrm{g}}\cos(y_{\mathrm{g}}), \qquad \dot{y}_{\mathrm{g}} = \omega_{\mathrm{g}}. \quad (7.2)$$

Our aim is to express the coupled hull and gyroscope control system as a linear graph and illustrate how the energy-balance method applies. As we shall see, for a graph-theoretic treatment it is important to distinguish between whether coupling between hull and gyroscope is linearised for small y_{g}, meaning that $\cos(y_{\mathrm{g}})$ is replaced by one, or not. Unsurprisingly, the linearised coupling case is more straightforward, and we consider it first.

7.3. Linearised coupling

If the variable y_{g} is assumed small, so that $\cos(y_{\mathrm{g}})$ is replaced by one, then the variable y_{g} may be omitted from 7.2 and the coupling between the hull and gyroscope is via a transducer, as

$$\begin{pmatrix} F_{\mathrm{hull}\to\mathrm{gyro}} \\ F_{\mathrm{gyro}\to\mathrm{hull}} \end{pmatrix} = \begin{pmatrix} 0 & -\eta \\ \eta & 0 \end{pmatrix} \begin{pmatrix} \omega_{\mathrm{h}} \\ \omega_{\mathrm{g}} \end{pmatrix} = G \begin{pmatrix} \omega_{\mathrm{h}} \\ \omega_{\mathrm{g}} \end{pmatrix}.$$

We initially give separate graphs for the hull and the gyroscope. Since the transducer is a gyrator, we need to choose dual analogies in order to merge the graphs, as discussed in Section 3.4. For the hull system, we choose angular velocity differences as the across variables and torques as the through variables — the mobility analogy. This gives the graph in Figs. 7.1(a) and a description of the edges appears in Table 7.1. Consequently, we use the impedance analogy for the gyroscope, so that angular velocity differences are through variables and torques are across variables. This gives the linear graph for the gyroscope system shown in Fig. 7.1(b) with a description of edges given in Table 7.2. By scaling the variables of one of the graphs by η, we can combine the two graphs into one, as depicted in Fig. 7.1(c). For simplicity for the remainder of the example, we set $\eta = 1$.

In the following subsections we apply the energy-balance method for versions of the wave energy converter model considered.

7.3.1. Only the hull damped

Assume first that the radiation system is absent and the gyroscope is undamped. Consequently, the R_2 and R_3 edges are absent from the graph in Fig. 7.1(c) and instead we obtain the subgraph appearing in Fig. 7.1(d). The energy-balance method gives that the objective is to minimise

$$\int_{t_0}^{t_1} A_{\mathrm{e}}T_{\mathrm{e}} + A_{R_1}T_{R_1}\,\mathrm{d}t,$$

subject to the constitutive relationship (representing the nonlinear damping of the hull)

$$T_{R_1} = d_{\mathrm{h}}|A_{R_1}|A_{R_1} =: q_1(A_{R_1}) \text{ (from the green dissipator edge)}, \quad (7.3)$$

the across equation

$$A_{\mathrm{e}} = A_{R_1} \qquad \text{(from the single green face)},$$

and we recall that T_{e} is externally given.

As with some of the earlier examples considered, since the optimal control problem obtained by the energy-balance method only involves algebraic equations, it can be solved by pointwise minimisation of the integrand. For which purpose, a convenient choice for the new independent variable is A_{R_1}, the angular velocity of the hull. We can write the integrand in terms of this variable and the given T_{e}, the torque imposed by the incoming waves, as

$$A_{\mathrm{e}}T_{\mathrm{e}} + A_{R_1}T_{R_1} = A_{R_1}\big(T_{\mathrm{e}} + q_1(A_{R_1})\big).$$

Differentiating the above and setting equal to zero, a necessary condition for a minimiser is that A_{R_1} and T_{e} satisfy:

$$0 = T_{\mathrm{e}} + q_1(A_{R_1}) + A_{R_1}q_1'(A_{R_1}) =: T_{\mathrm{e}} + r_1(A_{R_1}).$$

Inverting the function r_1 leads to the angular velocity of the hull as a function of the torque of the incoming wave. A straightforward calculation shows that $r_1(x) = 3q_1(x)$, so that

$$T_{\mathrm{e}} = -3q_1(A_{R_1}) = -3d_{\mathrm{h}}|A_{R_1}|A_{R_1},$$

which inverts to give

$$A_{R_1} = -\mathrm{sign}(T_{\mathrm{e}})\sqrt{\frac{|T_{\mathrm{e}}|}{3d_{\mathrm{h}}}}.$$

As usual, once the optimal control problem for the green subgraph is solved, we use the remaining equations to determine the remaining variables.

7.3.2. Including the radiation system

Including the radiation system corresponds to incorporating the R_2 edge in Figs. 7.1(c) and 7.1(d). The energy-balance method now gives that the objective is to minimise

$$\int_{t_0}^{t_1} A_{\mathrm{e}}T_{\mathrm{e}} + T_{R_1}A_{R_1} + T_{R_2}A_{R_2}\,\mathrm{d}t.$$

We have the across equations

$$A_{\mathrm{e}} = A_{R_1} = A_{R_2} \qquad \text{(from the two green faces)},$$

and the nonlinear damping of the hull (7.3), as before. The term T_{R_2} is given in terms of A_{R_1} by the radiation system

$$\dot{z} = A_R z + B_R A_{R_1}, \qquad T_{R_2} = C_R z.$$

Therefore, we have an optimal control problem with input A_{R_1} and dynamic state variable z. Once this is solved, the other variables can be determined from the remaining equations.

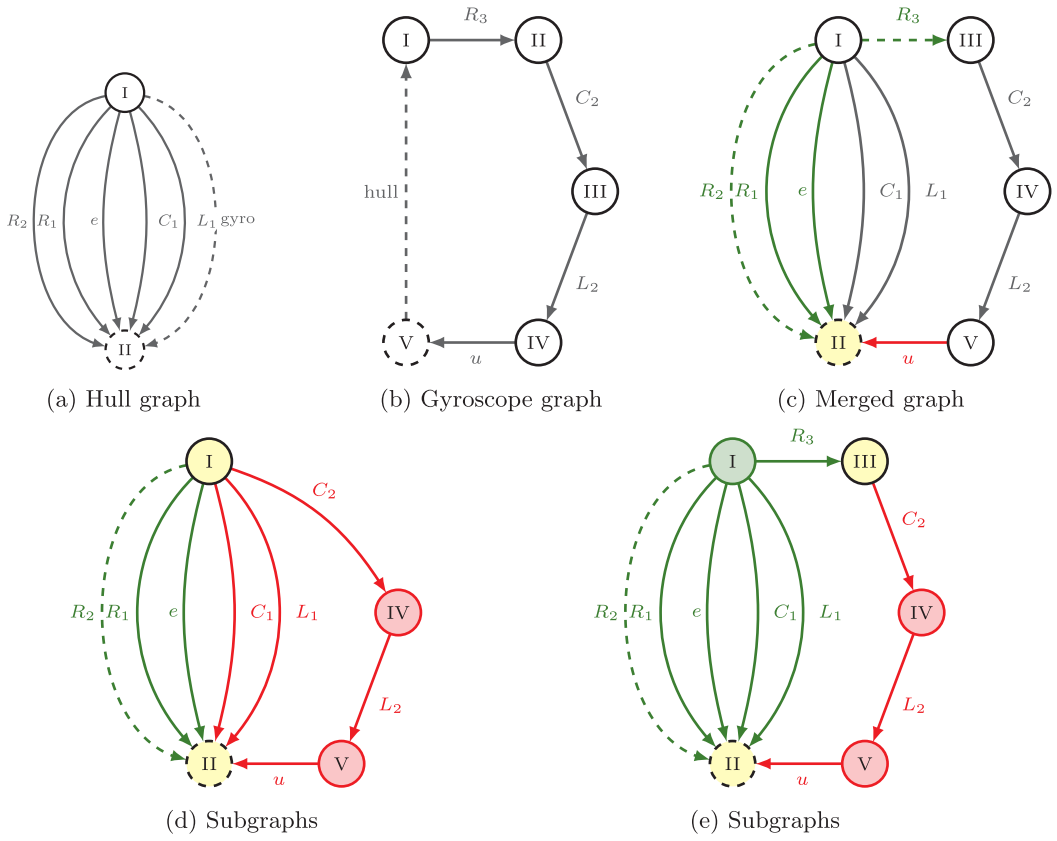

Fig. 7.1. Linear graphs for wave energy converter with linearised coupling. Dashed green edges are absent when corresponding damping term is omitted, and present otherwise. Yellow nodes are shared and the dashed node is ground. (a) Hull graph (with mobility analogy) (b) Gyroscope graph (with impedance analogy) (c) Merged wave energy converter graph. (d) and (e) Subgraph and complement for undamped and damped gyroscope, respectively.

7.3.3. *Including all damping*

When we assume that both the hull and the gyroscope are damped, then we obtain the subgraph in Fig. 7.1(e). Observe that the C_1 and L_1 edges, corresponding to the stiffness and inertia of the hull, respectively, must be included in the green subgraph in order that the green and red subgraphs share only two vertices. The energy balance method proceeds as before. In light of the green subgraph in Fig. 7.1(e), the new optimal control problem is subject to one through equation and four across equations (corresponding to the one green vertex and four green faces, respectively), as well as two algebraic constitutive relationships from the dissipator edges R_1 and R_3, the dynamic dissipator equation from the radiation system, edge R_2, and two dynamic constitutive relationships from the accumulator edges L_1 and C_1.

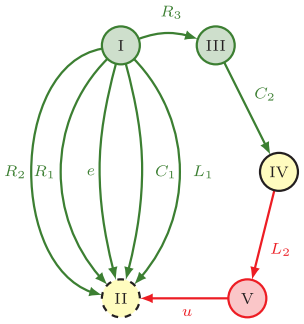

Fig. 7.2. The wave energy subgraph with nonlinear coupling when both the hull and gyroscope are damped.

7.4. *Nonlinear coupling*

If the coupling is nonlinear, then the term $\cos(y_g)$ appears in 7.2, particularly in the coupling terms between hull and gyroscope, where y_g is the position of the gyroscope. Therefore, to merge the hull and gyroscope graphs a nonlinear, dynamic gyrator is required, of the form

$$\begin{pmatrix} F_{\text{hull}\to\text{gyro}} \\ F_{\text{gyro}\to\text{hull}} \end{pmatrix} = \begin{pmatrix} 0 & -\eta\cos(y_g) \\ \eta\cos(y_g) & 0 \end{pmatrix} \begin{pmatrix} \omega_h \\ \omega_g \end{pmatrix} = G(y_g) \begin{pmatrix} \omega_h \\ \omega_g \end{pmatrix}, \qquad \dot{y}_g = \omega_g \,.$$

Such a component falls outside of the scope of the graph-theoretic treatment of control systems considered currently, and is beyond the scope of the present contribution. Some heuristics are available, however. To incorporate the nonlinear coupling requires including the variable y_g and solving the differential equation $\dot{y}_g = \omega_g$. For the gyroscope, ω_g is a through variable, so this equation is essentially an across accumulator equation. Thus, even with the nonlinear coupling, we can view the merged graphs as those in Figs. 7.1(c), 7.1(d) and 7.1(e) only where the edge C_2 is replaced by an edge corresponding to the gyroscope stiffness *and* this additional across accumulator equation.

Since the C_2 edge is not included when the gyroscope is assumed undamped, as considered in Sections 7.3.1 and 7.3.2, the energy-balance method described there still applies. When the gyroscope is assumed damped then we can include the across accumulator edge, labelled C_2, into the green subgraph, as in Fig. 7.2. Although the graph-theoretic approach presented earlier formally does not apply, the graph is still useful in determining a smaller optimal control problem to be solved.

8. Extensions and including constraints

Here we briefly comment on extensions to the energy-balance method.

First, we have focussed so far on control systems expressed as linear graphs which contain a single external edge and a single control edge. The energy-balance equation (4.2) generalises to multiple external edges, and multiple controls, and becomes

$$E(t_1) - E(t_0) + \sum_{\substack{\text{PTO}\\ \text{control}}} \int_{t_0}^{t_1} A_u T_u \,\mathrm{d}t = - \sum_{\substack{\text{other}\\ \text{control}}} \int_{t_0}^{t_1} A_u T_u - \sum_{\text{external}} \int_{t_0}^{t_1} A_e T_e \,\mathrm{d}t - \sum_{\text{dissipator}} \int_{t_0}^{t_1} A_k T_k \,\mathrm{d}t\,, \tag{8.1}$$

where PTO denotes power take-off. The derivation of (8.1) is analogous to that of (4.2), starting from the integrated version of Tellegen's theorem (4.4). In principle, the same ideas underpinning the energy-balance method apply here — maximising the left-hand side of (8.1) is equivalent to maximising the right-hand side of (8.1), which becomes the new performance objective. The problem remains of extracting an appropriate, as small as possible, subgraph to

(a) permit the optimisation of, and;
(b) uniquely determine all the (remaining) variables of

the right-hand side of (8.1). It is beyond the scope of the present contribution to investigate when such a graph-splitting procedure is practicable. Observe that the additional generality afforded by (8.1) as compared to (4.2) was not required in the examples presented in Sections 5–7.

Second, the optimal control problems considered presently are not subject to any input- or state-constraints. Such constraints are likely to be present in all real-world renewable energy generation contexts, although again we reiterate that the energy-balance method provides a theoretical maximum against which other control strategies, including those with constraints, may be compared.

The energy-balance method may be adjusted to incorporate state-constraints as follows. Essentially, any constrained edge variable in the original optimal control problem must be included in the green subgraph — as these are the variables which appear in, and hence are determined by, the new optimisation problem. Constraints may then be treated by classical optimal control tools, such as versions of the Pontryagin Principle. Since it is often convenient to take a flexible interpretation of the roles of variables in the new optimal control problem, whether an original variable receives a state or input (independent variable) constraint will vary between applications. Currently, the (PTO) control edge variable is never placed in the green subgraph, and so traditional input constraints cannot be accommodated by this adjustment. It is worth commenting that it may be the case that the control edge variables determined by the (possibly constrained) energy-balance method may satisfy its constraints and, in this case, is optimal even for the constrained problem. However, this may not happen and, in which case, the underpinning ideas of using (4.2) or (8.1) to obtain a new optimal control problem may still be applicable for "large" problems with certain constraints.

Third, we reiterate that we have not explored in depth how to perform the graph-splitting procedure, an essential ingredient of the energy-balance method. For small graphs, a visual inspection and colouring suffices, but this will prove intractable for "large" examples. We note here that seeking a decomposition of edges of the original linear graph corresponds to seeking a decomposition of vertices of the corresponding "graph" with vertices and nodes interchanged. Mathematically, this corresponds to viewing $M^\top$ as an incidence matrix which will lead to a hypergraph in general — where a single (hyper)edge may connect to more than two vertices. Separating a graph into two distinct sets of vertices is called a *cut*, and graph cutting problems are very well studied. Extensions to the setting of cuts for hypergraphs have been considered (see, for example [72]) and it may be possible to reformulate the current graph-splitting problem as a minimum cut problem for the associated hypergraph.

Fourth, and finally, we conjecture that the solution of the optimal control problem considered here, namely to maximise

$$E(t_1) - E(t_0) + \int_{t_0}^{t_1} A_u T_u \,\mathrm{d}t\,,$$

subject to the control system (CS) — which is the focus of the energy-balance method — is in fact the singular control related to the following constrained optimal problem: namely, to maximise purely the extracted energy, that is,

$$\int_{t_0}^{t_1} A_u T_u \,\mathrm{d}t\,,$$

(note no boundary energy terms) subject to the control system (CS) *and* the control constraint $X_{\min} \le X_u(t) \le X_{\max}$, where $X_u = A_u$ or T_u is the control variable. In general, this latter problem will have bang-singular (also known as bang-singular-bang) solutions, where the optimal control either rides the constraints (bang), or equals the singular solution. Establishing the validity of this conjecture shall also be the subject of future work.

9. Summary

The energy-balance method for simplifying optimal control problems associated with renewable energy conversion has been presented. The method applies to control systems specified by linear graphs in terms of across and through edge variables, with a number of fixed edge types (denoting lumped, one-port two-terminal element types) and essentially uses Tellegen's theorem to rewrite the extracted energy in terms of the supplied energy and dissipated energy, Eq. (4.2). We called this expression the energy-balance equation. A graph-splitting procedure has been proposed for solving the original optimal control problem by identifying fewer, but sufficiently many, variables to optimise the new performance criterion — the right-hand side of the energy-balance equation. One strength of the energy-balance method is that elements do not need to be ideal — they may be nonlinear or, in certain cases, dynamic. The energy-balance method does not specify the optimisation method to be used to the solve resulting simpler optimal control problem, and this choice may be made situationally or according to user preference.

By specifying control systems in terms of linear graphs and using transducers (transformers and gyroscopes), the energy-balance method may be applied to control systems spanning multiple energy domains, such as mechatronic systems. For instance, in the context of wave energy, oscillating water column devices span fluid (via water and air), mechanical (via turbines), and electrical (via generators) domains. Consequently, the method facilitates optimisation at the level of the whole control system. The method has been illustrated via examples from solar, wind and wave energy across Sections 5–7. From a practical engineering perspective, we recommend that the method is considered whenever an optimal control of a renewable energy converter is implemented, as it may well simplify the computational complexity of the overall problem.

One feature which emerges from the study is the importance of the *structure* of the control system in determining the variables which are key to maximising the extracted energy. This structure is seemingly most easily visualised and understood graphically rather than, say, by a traditional state–space representation. For example, on the one hand, when no energy storage (accumulator) elements are present in the subgraph obtained by the graph-splitting procedure (recall, termed the green subgraph), then the resulting performance criterion is static, that is, subject only to algebraic constraints. Therefore, it may be maximised by pointwise maximisation of the integrand — essentially by elementary calculus methods. In other words, here the need for

classical optimal control techniques is obviated. On the other hand, including additional accumulator edges in the red subgraph (recall, the complementary subgraph) *does not* change the performance objective associated with the energy-balance method or its solution. Of course, the variables associated with the red subgraph, which includes the original control variable, do depend on the red subgraph, and so change as the structure and/or composition of this subgraph changes.

The energy-balance method determines an optimal control over a finite (possibly short) prediction interval, here denoted $[t_0, t_1]$. In practice, to use this method continuously in time requires piecing together multiple, successive prediction intervals. We comment that a key feature of optimal control problems in renewable energy contexts is accurately forecasting the external variables over the prediction interval, such as the incoming wave profile in wave energy applications; see, for example [67]. This challenge (or opportunity, depending on outlook) is still present in the energy-balance method.

Some extensions and current limitations of the method have been discussed in Section 8, notably on how the method may generalise to optimal control problems with multiple control and external sources, and the extent to which constraints may be included. Exploring these directions further shall be the subject of future studies. Furthermore, bond graph modelling, originating in the work of Paynter [73], with recent texts including [74], is recommended by its proponents as a powerful and widely applicable framework for control systems spanning multiple energy domains. Formulating the energy-balance method in terms of bond graphs rather than linear graphs may well be possible, and shall also be subject of future work.

Declaration of competing interest

The authors declare that they have no known competing financial interests or personal relationships that could have appeared to influence the work reported in this paper.

Data availability

No data was used for the research described in the article.

Acknowledgements

Chris Guiver's contribution to this work has been supported by a Personal Research Fellowship from the Royal Society of Edinburgh (RSE), award reference 2168. Chris Guiver expresses gratitude to the RSE for the financial support.

References

[1] United Nations Environment Programme, Emissions Gap Report 2022: The Closing Window — Climate Crisis Calls for Rapid Transformation of Societies, Tech. Rep., Nairobi, 2022.
[2] B.D. Tellegen, A general network theorem with applications, Philips Res. Rep. 7 (1952) 256–269.
[3] D. Rowell, D.N. Wormley, System Dynamics: An Introduction, Prentice Hall, New Jersey, 1997.
[4] C.W. De Silva, Modeling of Dynamic Systems with Engineering Applications, second ed., CRC Press, Boca Raton, FL, 2022.
[5] I.J. Busch-Vishniac, Electromechanical Sensors and Actuators, Springer, New York, 1998.
[6] A. Lenk, R.G. Ballas, R. Werthschützky, G. Pfeifer, Electromechanical systems in microtechnology and mechatronics: electrical, mechanical and acoustic networks, their interactions and applications, in: Microtechnology and MEMS, Springer-Verlag, Berlin, 2010.
[7] I. Sinclair, Sensors and Transducers, third ed., Newnes, Oxford, 2001.
[8] J.V. Ringwood, Wave energy control: status and perspectives 2020, IFAC-Pap. 53 (2) (2020) 12271–12282.
[9] F. Clarke, Functional Analysis, Calculus of Variations and Optimal Control, in: Graduate Texts in Mathematics, vol. 264, Springer, London, 2013.
[10] D. Liberzon, Calculus of Variations and Optimal Control Theory, Princeton University Press, 2011.
[11] A. Seierstad, K. Sydsaeter, Optimal Control Theory with Economic Applications, in: Advanced Textbooks in Economics, vol. 24, North Holland, Amsterdam, 1987.
[12] O. Hernández-Lerma, L.R. Laura-Guarachi, S. Mendoza-Palacios, D. González-Sánchez, An Introduction to Optimal Control Theory—The Dynamic Programming Approach, in: Texts in Applied Mathematics, vol. 76, Springer, Cham, 2023.
[13] J.T. Betts, Practical Methods for Optimal Control and Estimation using Nonlinear Programming, Second Edition, second ed., Society for Industrial and Applied Mathematics, Philadelphia, PA, 2010.
[14] Y. Nesterov, Lectures on Convex Optimization, second ed., in: Springer Optimization and Its Applications, vol. 137, Springer, Cham, 2018.
[15] J. Nocedal, S.J. Wright, Numerical Optimization, second ed., in: Springer Series in Operations Research and Financial Engineering, Springer, New York, 2006.
[16] S. Zou, O. Abdelkhalik, R. Robinett, G. Bacelli, D. Wilson, Optimal control of wave energy converters, Renew. Energy 103 (2017) 217–225.
[17] J. Falnes, Ocean Waves and Oscillating Systems: Linear Interactions Including Wave-Energy Extraction, Cambridge University Press, Cambridge, UK, 2002.
[18] A. Clément, A. Babarit, Discrete control of resonant wave energy devices, Phil. Trans. R. Soc. A 370 (1959) (2012) 288–314.
[19] W.A. Blackwell, Mathematical Modeling of Physical Networks, Macmillan Publishing Company, New York NY, 1968.
[20] S.P. Chan, S.Y. Chan, S.G. Chan, Analysis of Linear Networks and Systems, Addison-Wesley Publishing Company, Reading MA, 1972.
[21] H.E. Koenig, Y. Tokad, H.K. Kesavan, Analysis of Discrete Physical Systems, McGraw-Hill Book Company, New York, NY, 1967.
[22] B. Bollobás, Modern Graph Theory, in: Graduate Texts in Mathematics, vol. 184, Springer, New York, 1998.
[23] C. Guiver, H. Logemann, M.R. Opmeer, Transfer functions of infinite-dimensional systems: positive realness and stabilization, Math. Control Signals Systems 29 (4) (2017) 1–61.
[24] F.A. Firestone, A new analogy between mechanical and electrical systems, J. Acoust. Soc. Am. 4 (3) (1933) 249–267.
[25] H.M. Trent, Isomorphisms between oriented linear graphs and lumped physical systems, J. Acoust. Soc. Am. 27 (3) (1955) 500–527.
[26] M.C. Smith, Synthesis of mechanical networks: the inerter, IEEE Trans. Automat. Control 47 (10) (2002) 1648–1662.
[27] N. Jenkins, J. Ekanayake, Renewable Energy Engineering, Cambridge University Press, Cambridge, UK, 2017.
[28] S. Kouro, J.I. Leon, D. Vinnikov, L.G. Franquelo, Grid-connected photovoltaic systems: An overview of recent research and emerging pv converter technology, IEEE Ind. Electron. Mag. 9 (1) (2015) 47–61.
[29] M. Malinowski, J.I. Leon, H. Abu-Rub, Solar photovoltaic and thermal energy systems: Current technology and future trends, Proc. IEEE 105 (11) (2017) 2132–2146.
[30] T. Sadamoto, A. Chakrabortty, T. Ishizaki, J. i. Imura, Dynamic modeling, stability, and control of power systems with distributed energy resources: Handling faults using two control methods in tandem, IEEE Control Syst. Mag. 39 (2) (2019) 34–65.
[31] A.R. Reisi, M.H. Moradi, S. Jamasb, Classification and comparison of maximum power point tracking techniques for photovoltaic system: A review, Renew. Sustain. Energy Rev. 19 (2013) 433–443.
[32] A. Anurag, S. Bal, S. Sourav, M. Nanda, A review of maximum power-point tracking techniques for photovoltaic systems, Int. J. Sustain. Energy 35 (5) (2016) 478–501.
[33] D. Verma, S. Nema, A. Shandilya, S.K. Dash, Maximum power point tracking (MPPT) techniques: Recapitulation in solar photovoltaic systems, Renew. Sustain. Energy Rev. 54 (2016) 1018–1034.
[34] A.O. Baba, G. Liu, X. Chen, Classification and evaluation review of maximum power point tracking methods, Sustain. Futures 2 (2020) 100020.
[35] M.F. Jalil, S. Khatoon, I. Nasiruddin, R. Bansal, Review of PV array modelling, configuration and MPPT techniques, Int. J. Model. Simul. 42 (4) (2022) 533–550.
[36] L. Mitra, U.K. Rout, Performance analysis of a new high gain dc–dc converter interfaced with solar photovoltaic module, Renew. Energy Focus 19 (2017) 63–74.
[37] A. Raj, S.R. Arya, J. Gupta, Solar PV array-based DC–DC converter with MPPT for low power applications, Renew. Energy Focus 34 (2020) 109–119.
[38] M.G. Villalva, J.R. Gazoli, E. Ruppert Filho, Comprehensive approach to modeling and simulation of photovoltaic arrays, IEEE Trans. Power Electron. 24 (5) (2009) 1198–1208.
[39] A. Mohapatra, B. Nayak, P. Das, K.B. Mohanty, A review on MPPT techniques of PV system under partial shading condition, Renew. Sustain. Energy Rev. 80 (2017) 854–867.
[40] M. Kermadi, Z. Salam, A.M. Eltamaly, J. Ahmed, S. Mekhilef, C. Larbes, E.M. Berkouk, Recent developments of MPPT techniques for PV systems under partial shading conditions: a critical review and performance evaluation, IET Renew. Power Gener. 14 (17) (2020) 3401–3417.
[41] IEA, Wind Electricity, Tech. Rep., IEA, Paris, 2022, Available from https://www.iea.org/reports/wind-electricity, License: CC BY 4.0.
[42] J. Slootweg, W. Kling, Modelling wind turbines for power system dynamics simulations: an overview, Wind Eng. 28 (1) (2004) 7–25.

[43] V. Thapar, G. Agnihotri, V.K. Sethi, Critical analysis of methods for mathematical modelling of wind turbines, Renew. Energy 36 (11) (2011) 3166–3177.
[44] K.E. Johnson, L.Y. Pao, M.J. Balas, L.J. Fingersh, Control of variable-speed wind turbines: standard and adaptive techniques for maximizing energy capture, IEEE Control Syst. Mag. 26 (2006) 70–81.
[45] E.J.N. Menezes, A.M. Araújo, N.S.B. Da Silva, A review on wind turbine control and its associated methods, J. Clean. Prod. 174 (2018) 945–953.
[46] J.G. Njiri, D. Söffker, State-of-the-art in wind turbine control: Trends and challenges, Renew. Sustain. Energy Rev. 60 (2016) 377–393.
[47] J.V. Ringwood, S. Simani, Overview of modelling and control strategies for wind turbines and wave energy devices: Comparisons and contrasts, Annu. Rev. Control 40 (2015) 27–49.
[48] F.D. Bianchi, H. De Battista, R.J. Mantz, Wind Turbine Control Systems: Principles, Modelling and Gain Scheduling Design, in: Advances in Industrial Control, Springer-Verlag, London, 2007.
[49] W. Yang, P.J. Tavner, C.J. Crabtree, Y. Feng, Y. Qiu, Wind turbine condition monitoring: technical and commercial challenges, Wind Energy 17 (5) (2014) 673–693.
[50] K. Kong, K. Dyer, C. Payne, I. Hamerton, P.M. Weaver, Progress and trends in damage detection methods, maintenance, and data-driven monitoring of wind turbine blades–a review, Renew. Energy Focus (2022).
[51] X. Zhao, G. Weiss, Strong stabilisation of a wind turbine tower model in the plane of the turbine blades, Internat. J. Control 87 (10) (2014) 2027–2034.
[52] T. Sadamoto, A. Chakrabortty, T. Ishizaki, J. i. Imura, Ynamic modeling, stability, and control of power systems with distributed energy resources, IEEE Control Syst. 39 (2) (2019) 34–65.
[53] P.I. Girsang, J.S. Dhupia, E. Muljadi, M. Singh, L.Y. Pao, Gearbox and drivetrain models to study dynamic effects of modern wind turbines, in: 2013 IEEE Energy Conversion Congress and Exposition, 2013, pp. 874–881.
[54] B. Drew, A.R. Plummer, M.N. Sahinkaya, A review of wave energy converter technology, Proc. Inst. Mech. Eng. A 223 (2009) 887–902.
[55] T. Aderinto, H. Li, Ocean wave energy converters: Status and challenges, Energies 11 (5) (2018) 1250.
[56] E. Rusu, F. Onea, A review of the technologies for wave energy extraction, Clean Energy 2 (1) (2018) 10–19.
[57] M. Rosati, J. Henriques, J. Ringwood, Oscillating-water-column wave energy converters: A critical review of numerical modelling and control, Energy Convers. Manag. X (2022) 100322.
[58] B. Guo, T. Wang, S. Jin, S. Duan, K. Yang, Y. Zhao, A review of point absorber wave energy converters, J. Mar. Sci. Eng. 10 (10) (2022) 1534.
[59] N. Tom, Review of Wave Energy Converter Power Take-Off Systems, Testing Practices, and Evaluation Metrics, Tech. Rep, National Renewable Energy Lab.(NREL), Golden, CO (United States), 2022.
[60] J. Xie, L. Zuo, Dynamics and control of ocean wave energy converters, Int. J. Dyn. Control 1 (2013) 262–276.
[61] J.V. Ringwood, G. Bacelli, F. Fusco, Energy-maximizing control of wave-energy converters: The development of control system technology to optimize their operation, IEEE Control Syst. Mag. 34 (5) (2014) 30–55.
[62] N. Faedo, S. Olaya, J.V. Ringwood, Optimal control, MPC and MPC-like algorithms for wave energy systems: An overview, IFAC J. Syst. Control 1 (2017) 37–56.
[63] U.A. Korde, J. Ringwood, Hydrodynamic Control of Wave Energy Devices, Cambridge University Press, Cambridge, 2016.
[64] K. Koca, A. Kortenhaus, H. Oumeraci, B. Zanuttigh, E. Angelelli, M. Cantu, R. Suffredini, G. Franceschi, Recent advances in the development of wave energy converters, in: 9th European Wave and Tidal Energy Conference, EWTEC, 2013, pp. 2–5.
[65] J. Falnes, A. Kurniawan, Fundamental formulae for wave-energy conversion, R. Soc. Open Sci. 2 (3) (2015) 140305.
[66] C. Windt, N. Faedo, M. Penalba, F. Dias, J.V. Ringwood, Reactive control of wave energy devices–the modelling paradox, Appl. Ocean Res. 109 (2021) 102574.
[67] Y. Peña-Sanchez, C. Windt, J. Davidson, J.V. Ringwood, A critical comparison of excitation force estimators for wave-energy devices, IEEE Trans. Control Syst. Technol. 28 (6) (2019) 2263–2275.
[68] X. Dong, Y. Li, D. Li, F. Cao, X. Jiang, H. Shi, A state-of-the-art review of the hybrid wind-wave energy converter, Prog. Energy 4 (2022) 042004.
[69] H.A. Said, J.V. Ringwood, Grid integration aspects of wave energy—overview and perspectives, IET Renew. Power Gener. 15 (14) (2021) 3045–3064.
[70] M. Bonfanti, A. Hillis, S.A. Sirigu, P. Dafnakis, G. Bracco, G. Mattiazzo, A. Plummer, Real-time wave excitation forces estimation: An application on the ISWEC device, J. Mar. Sci. Eng. 8 (10) (2020) 825.
[71] T. Perez, P.D. Steinmann, Analysis of ship roll gyrostabiliser control, IFAC Proc. 42 (18) (2009) 310–315, 8th IFAC Conference on Manoeuvring and Control of Marine Craft.
[72] N. Veldt, A.R. Benson, J. Kleinberg, Hypergraph cuts with general splitting functions, SIAM Rev. 64 (3) (2022) 650–685.
[73] H.M. Paynter, Analysis and Design of Engineering Systems, MIT Press, Cambridge, MA, 1961.
[74] W. Borutzky, Bond Graph Methodology: Development and Analysis of Multidisciplinary Dynamic System Models, Springer, London, 2010.